YGS Open File 2025-4

New geochronological and geochemical data for Permian rocks of the western Yukon-Tanana terrane, Klondike district, Yukon

M. Colpron[1], W.C. McClelland[2], S.J. Piercey[3], E.D.L. Kroeger[4], J.L. Crowley[5] and G.E. Gehrels[6]

[1] Yukon Geological Survey
[2] Department of Earth and Environmental Sciences, University of Iowa
[3] Department of Earth Sciences, Memorial University of Newfoundland
[4] Clemson University
[5] Boise State University
[6] Department of Geoscience, University of Arizona

Yukon

Published under the authority of the Department of Energy, Mines and Resources, Government of Yukon https://yukon.ca/en/department-energy-mines-resources.

Publié avec l'autorisation du Ministères de l'Énergie, des Mines et des Ressources du gouvernement du Yukon, https://yukon.ca/en/department-energy-mines-resources.

This, and other Yukon Geological Survey publications, may be obtained from:

Yukon Geological Survey
102-300 Main Street
Box 2703 (K-102)
Whitehorse, Yukon, Canada Y1A 2C6

email geology@gov.yk.ca

Visit the Yukon Geological Survey website at https://yukon.ca/en/science-and-natural-resources/geology.

In referring to this publication, please use the following citation:

Colpron, M., McClelland, W.C., Piercey, S.J., Kroeger, E.D.L., Crowley, J.L. and Gehrels, G.E., 2025. New geochronological and geochemical data for Permian rocks of the western Yukon-Tanana terrane, Klondike district, Yukon. Yukon Geological Survey, Government of Yukon, Open File 2025-4, 35 p. plus appendices.

Front cover: Exposure of Klondike Schist along French Gulch, locality 19MC018. Photo credit: Maurice Colpron, Yukon Geological Survey.

Yukon

YGS Open File
2025-4

New geochronological and geochemical data for Permian rocks of the western Yukon-Tanana terrane, Klondike district, Yukon

Maurice Colpron[1], William C. McClelland[2], Stephen J. Piercey[3],
Emma D.L. Kroeger[4], James L. Crowley[5] and George E. Gehrels[6]

[1] Yukon Geological Survey
[2] Department of Earth and Environmental Sciences, University of Iowa
[3] Department of Earth Sciences, Memorial University of Newfoundland
[4] Clemson University
[5] Boise State University
[6] Department of Geoscience, University of Arizona

Table of Contents

Abstract

New U-Pb zircon dates from Permian rocks of the Yukon-Tanana terrane in the Klondike district of western Yukon provide new constraints on timing of intrusions and deposition. The new data shows that significant Pb-loss affected zircon in metamorphic rocks of the Yukon-Tanana terrane. The new, high-precision CA-TIMS dating shows that all intrusions in the region are ca. 261 Ma and eliminate previous constraints on the Klondike orogeny. A review of lithogeochemical data and new Lu-Hf isotope data for zircon support development of the Klondike assemblage in back-arc to continental arc settings. New $^{40}Ar/^{39}Ar$ data for Permian metaplutonic rocks indicates cooling below 300-350°C in the Early Jurassic.

Plain language summary

This report presents new radiometric dates for metamorphic rocks of the Klondike district in western Yukon. The new data helps refine the timing of geological events in the Permian, about 260 million years ago, and shows that metamorphism was completed by the Early Jurassic, about 190–180 million years ago. A review of geochemical data for these rocks provides information about the plate tectonic setting in which they formed.

Introduction

The Yukon-Tanana terrane (Fig. 1) comprises metamorphosed sedimentary, volcanic and plutonic rocks ranging in age from Late Devonian to late Permian (Lopingian). It includes a lower metasedimentary succession (Snowcap assemblage) overlain by three unconformity-bounded arc/back-arc successions — the Late Devonian to Early Mississippian Finlayson assemblage, the Middle Mississippian to early Permian (Cisuralian) Klinkit assemblage, and the mid- to late Permian (Guadalupian to Lopingian) Klondike assemblage (Colpron et al., 2006). Arc successions of the Finlayson and Klinkit assemblages were deposited concurrently with development of the Slide Mountain back-arc ocean that separated Yukon-Tanana from the western Laurentian continental margin from Late Devonian to Cisuralian (Mortensen, 1992; Nelson et al., 2006; Colpron et al., 2007). Closure of the Slide Mountain Ocean in Guadalupian–Lopingian is recorded in a belt of high-pressure metamorphic rocks along the eastern edge of Yukon-Tanana terrane and the Klondike assemblage is generally interpreted to represent arc magmatism related with this phase of tectonic evolution. The Klondike assemblage comprises metavolcanic and metasedimentary rocks of the Klondike Schist (ca. 267–254 Ma) and associated metaplutonic rocks of the Sulphur Creek suite (ca. 265–255 Ma; Mortensen, 1990, 1992). Supra-subduction ophiolitic complexes of the Dawson–Clinton Creek assemblage (formerly assigned to the Slide Mountain terrane; e.g., Mortensen, 1992, 1996; Gordey and Makepeace, 2001; Colpron et al., 2016) were emplaced within the Yukon-Tanana terrane by hyper-extension ca. 265–264 Ma, preceding onset of magmatism in the Klondike assemblage (van Staal et al., 2018).

Rocks of the Yukon-Tanana terrane are generally deformed and metamorphosed to greenschist and amphibolite facies. These rocks are characterized by a penetrative dominant foliation and tight to isoclinal folds. Based on relationships in the Klondike district of western Yukon, it has been inferred that at least part of the penetrative deformation and metamorphism occurred in the Lopingian (Klondike orogeny, ca. 260–252 Ma; Beranek and Mortensen, 2011). This event was inferred to be related to the collisional Klondike orogeny, following closure of the Slide Mountain Ocean.

This report presents new U-Pb geochronological data for igneous and detrital zircons from Permian rocks of the Yukon-Tanana terrane in the Klondike district of western Yukon (Fig. 1). Uranium-lead zircon analyses were aimed at: 1) testing and refining age constraints on the timing of the Klondike orogeny; and 2) characterizing the source of metasedimentary rocks within the Klondike Schist. Samples were analyzed using a combination of laser ablation inductively coupled mass spectrometry (LA-ICPMS) and chemical abrasion thermal ionization mass spectrometry (CA-TIMS). Representative zircon grains were also analyzed for Lu-Hf isotopes by LA-ICPMS. Whole rock geochemical data from igneous rocks of the Klondike and Dawson–Clinton Creek assemblages are compiled (including previously unpublished analyses) and reviewed to characterize the magmatic affinities of these rocks. Finally, $^{40}Ar/^{39}Ar$ analyses of mica from a few igneous rock samples of the Sulphur Creek suite are also presented in this report.

This report presents the data that support more comprehensive interpretations and implications for the tectonic evolution of the northern Cordillera presented in Colpron et al. (2025).

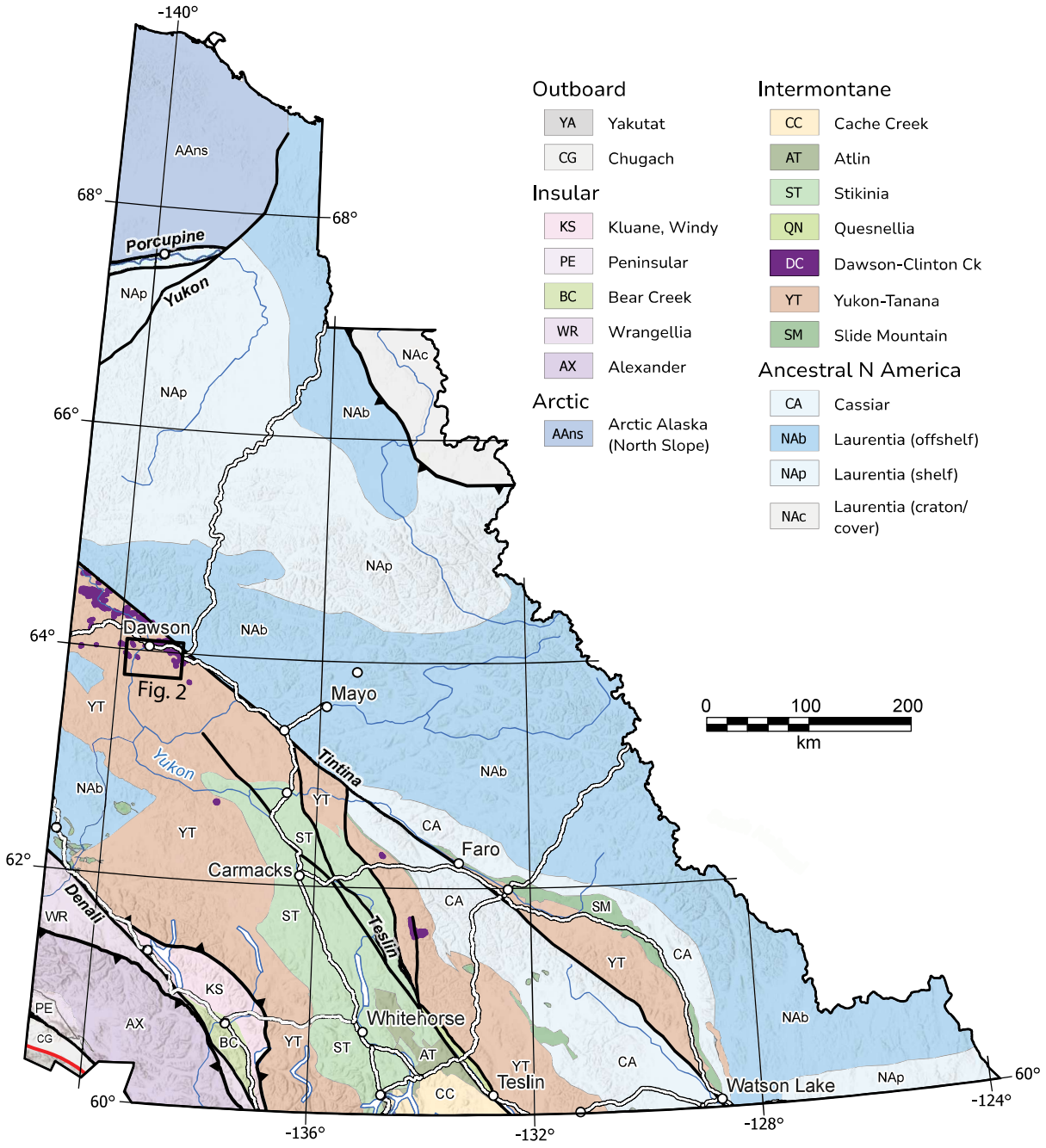

Figure 1. *Terrane map of Yukon showing the location of the Klondike study area in the Yukon-Tanana terrane (Yukon Geological Survey, 2024).*

Geology of the Klondike district

The Klondike district, south of Dawson, Yukon, is famous for the 1898 Gold Rush (Dawson, 1899, p. 7-9; McConnell, 1905). It is primarily underlain by rocks of the Yukon-Tanana terrane imbricated with greenstone–ultramafic rocks of the Dawson–Clinton Creek assemblage along a series of northeast-verging thrust faults (Fig. 2; Mortensen, 1988a, 1996; Gordey and Ryan, 2005; MacKenzie et al., 2008). In this region, the Yukon-Tanana terrane comprises mainly carbonaceous metasedimentary rocks of the Nasina assemblage (part of the regional Finlayson assemblage) and metavolcanic and metasedimentary rocks of the Klondike Schist. The Nasina

assemblage consists of fine-grained, carbonaceous schist and phyllite, micaceous quartzite, marble, and rare chlorite schist (Fig. 3a; Mortensen, 1988a, 1988b, 1996). West of Dawson, isolated occurrences of felsic schist (metavolcanic and/or metaplutonic) in carbonaceous phyllite of the Nasina assemblage have U-Pb zircon dates of ca. 361-348 Ma (Dusel-Bacon et al., 2006; Dusel-Bacon and Mortensen, 2023, 2024). Younger, felsic metaporphyry and schist intruding the Nasina assemblage west of Dawson were dated by U-Pb zircon ca. 263–253 Ma and indicate that Permian magmatism of the Klondike assemblage was constructed on older Late Devonian – Mississippian components of the Yukon-Tanana terrane (Dusel-Bacon and Mortensen, 2023, 2024). In the Klondike region, rocks of the Nasina assemblage occur in the footwall of the Hunker thrust to the north, and southwest of the Ninemile thrust (Fig. 2).

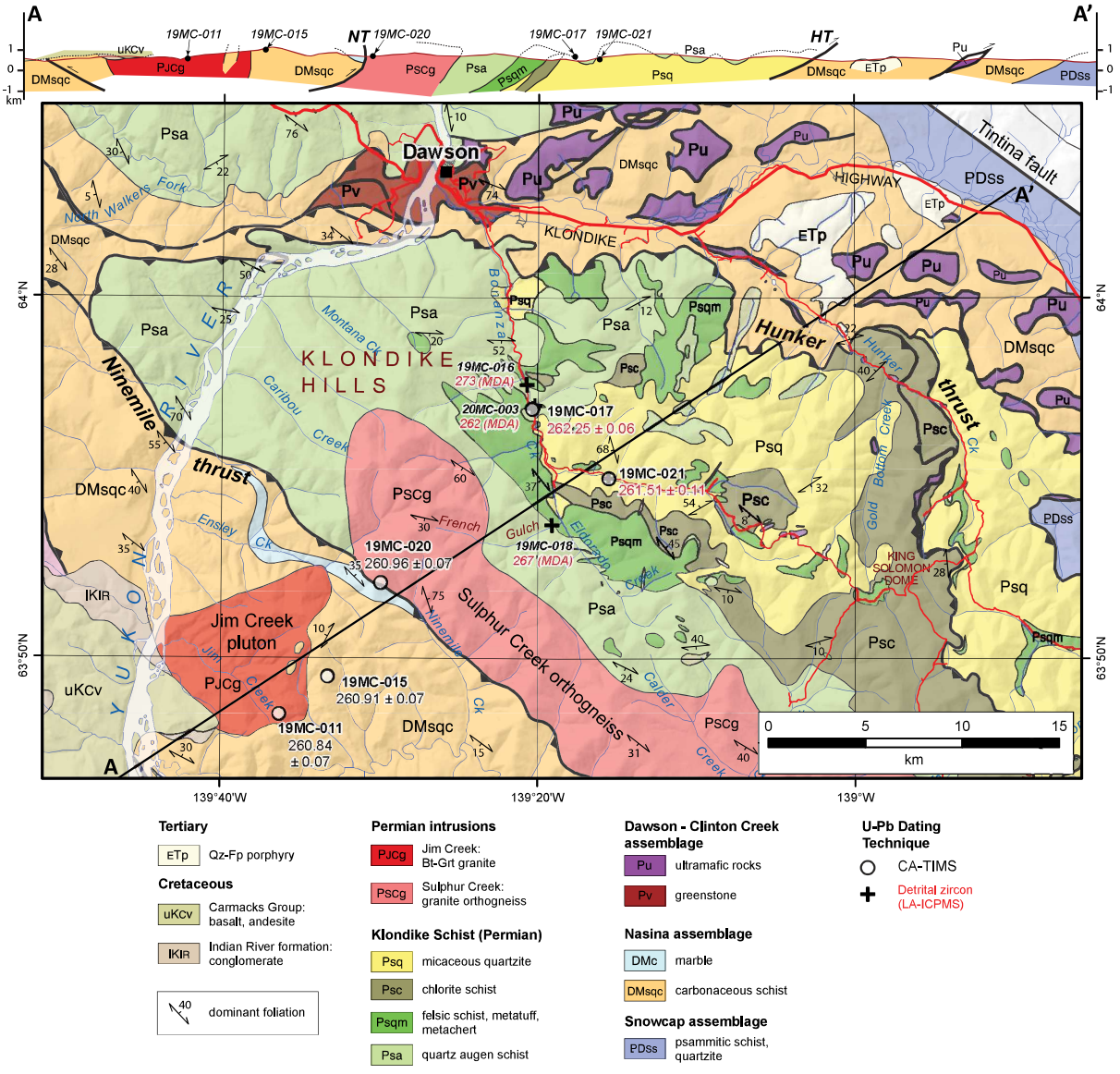

Figure 2. *Geological map of the Klondike region, western Yukon. Modified after Mortensen (1996). The location of samples dated by U-Pb zircon are symbolized by dating technique with ages in million years (Ma). Sample numbers are indicated for data presented in this study (Table 1). Igneous ages from this study are shown in black, while red font indicate detrital zircon maximum depositional ages (MDA). Errors (2σ) are shown for samples dated by CA-TIMS in this study (Table 1). Cross-section A-A' is shown at the top with approximate position of samples dated by CA-TIMS in this study. HT = Hunker thrust; NT = Ninemile thrust.*

The Klondike Schist occupies the structural panel between the Ninemile and Hunker thrusts and comprises four map units exposed on the flanks of a structural dome (Fig. 2; Mortensen, 1996). Quartz augen schist and gritty quartzite (Psa; Fig. 3b,c) occur at higher structural levels, in the footwall of the Ninemile thrust. These rocks are intercalated with and grades eastward into fine-grained quartz-feldspar-muscovite schist (metatuff?) and micaceous quartzite (Psqm; Fig. 3d,e), and into bands of chlorite schist (Psc) and micaceous quartzite (Psq; Fig. 3f) at lower structural levels (Fig. 2). Quartz augen schist of unit Psa is inferred to represent a subvolcanic sill complex to felsic metavolcanic rocks of Psqm (Mortensen, 1996). Unit Psa appears gradational into medium to coarse-grained, foliated quartz monzonite to granite, locally with K-feldspar augens, of the Sulphur Creek orthogneiss (Fig. 4a,b). Felsic metavolcanic rocks and quartz augen schist of the Klondike Schist in this region yielded U-Pb zircon dates ranging 263–253 Ma, while foliated quartz monzonite and granite of the Sulphur

Figure 3. a) *Strongly foliated carbonaceous schist and quartzite of the Nasina assemblage at the headwater of Ensley Creek.* ***b)*** *Quartzo-feldspathic schist, unit Psa, locality 19MC-017.* ***c)*** *Gritty quartzite, unit Psa, locality 20MC-003.* ***d****) Quartzite from unit Psqm, locality 19MC-016.* ***e)*** *Porphyroclastic muscovite-plagioclase-quartz-garnet-chlorite schist at the contact between units Psa and Psqm, locality 19MC-018.* ***f)*** *Quartz-mica schist, unit Psq, locality 19MC-021.*

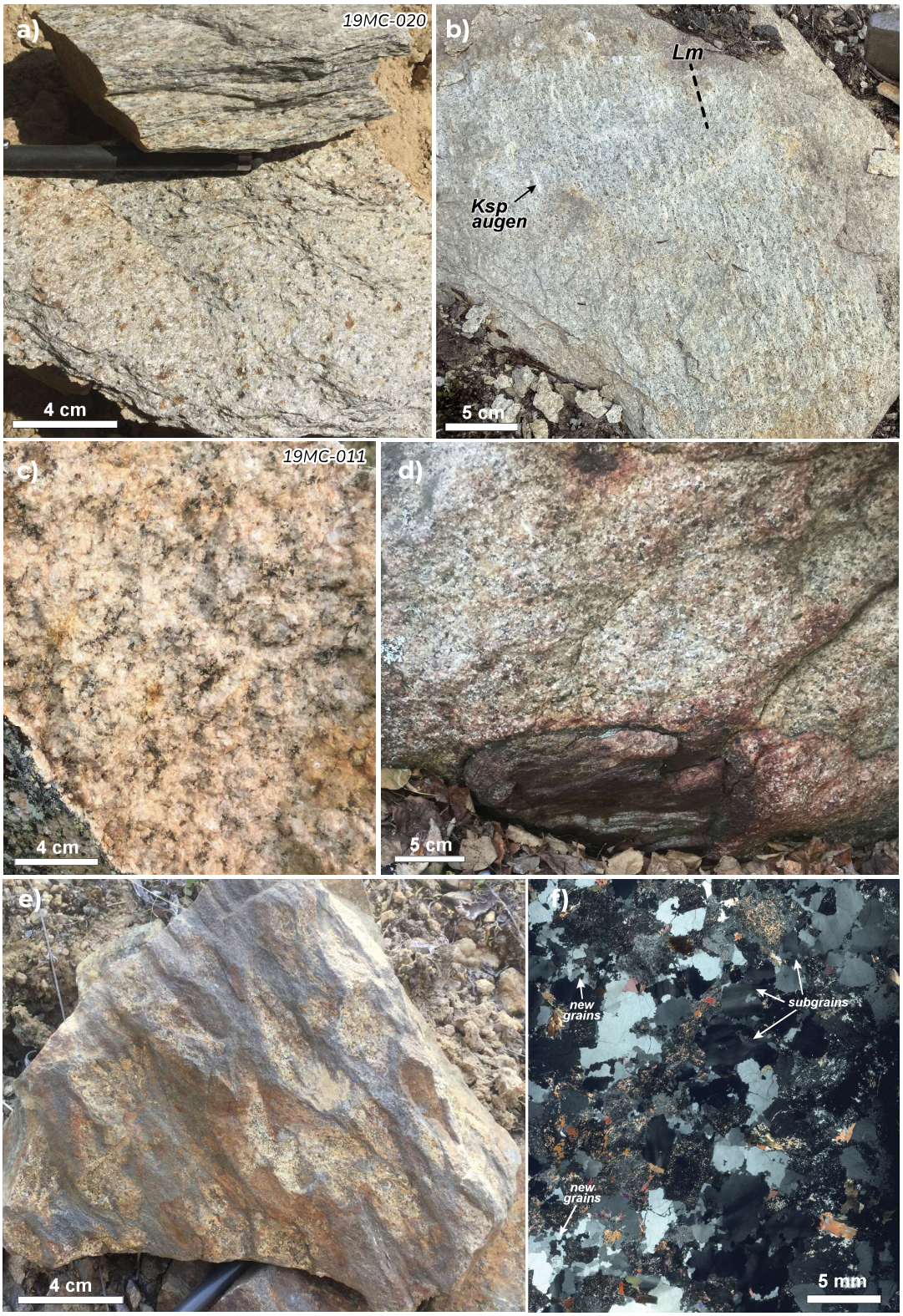

Figure 4. a) *Strongly foliated metagranite of the Sulphur Creek orthogneiss in proximity to the Ninemile thrust at locality 19MC-020. Hand sample (top) and outcrop surface (bottom).* ***b)*** *Lineated, K-feldspar augen granite, Sulphur Creek orthogneiss near the Ninemile thrust.* ***c)*** *Coarse-grained two-mica granite from the Jim Creek pluton, locality 19MC-011.* ***d****) Dike of two-mica granite with xenolith of foliated graphitic schist.* ***e)*** *Granite apophyses deformed with host schist along the eastern margin of the Jim Creek pluton.* ***f****) Scanned thin section (crossed polarized light) showing evidence of dislocation (subgrains) and recrystallization (new grains) in quartz near the margin of the Jim Creek pluton. Note incipient saussuritization of plagioclase.*

Creek orthogneiss has U-Pb zircon dates of 262–260 Ma (Fig. 2; Mortensen, 1990; Dusel-Bacon and Mortensen, 2023, 2024). Southwest of the Ninemile thrust, carbonaceous schist of the Nasina assemblage is intruded by two-mica (± garnet) granite of the Jim Creek pluton and related dikes that yielded U-Pb zircon dates ca. 260-252 Ma (Fig. 2; Beranek and Mortensen, 2011). The relationships surrounding the Jim Creek pluton are critical to interpretation of the Klondike orogeny. Beranek and Mortensen (2011, p. 7) describe the Jim Creek pluton and associated dikes as massive and undeformed with sharp contacts cutting the foliation in the Nasina schist (Fig. 4c,d). Our observations show that the contacts of the Jim Creek pluton are locally deformed along with the wall rock (Fig. 4e). Samples from apparently undeformed granite exhibit evidence of recrystallization and dislocation in thin section, including undulose extinction, subgrains, new quartz grains (Fig. 4f), and kinked biotite crystals.

Greenstone–ultramafic rocks of the Dawson–Clinton Creek assemblage occur mainly in the footwall of the Hunker thrust in this region (Fig. 2). Greenstone and variably serpentinized harzburgite are structurally intercalated with carbonaceous phyllite of the Nasina assemblage. A leucogabbro intruding the ultramafic rocks near Dawson yielded a U-Pb zircon date of 264 ± 4 Ma (van Staal et al., 2018).

U-Pb geochronology and Hf isotopes

Five samples of metasedimentary rocks from the Klondike Schist were analyzed for detrital zircon U-Pb by LA-ICPMS at the Arizona LaserChron Center (ALC), University of Arizona (Table 1; Appendix A). Three samples of (meta)plutonic rocks from the Sulphur Creek orthogneiss and Jim Creek pluton were analyzed for U-Pb zircon using a combination of LA-ICPMS and CA-TIMS at the Isotope Geology Laboratory, Boise State University (Table 1; Appendices B and C). Maximum depositional ages (MDA) were also determined by CA-TIMS at the Isotope Geology Laboratory, Boise State University for two of the Klondike Schist samples (Appendix C). Finally, Lu-Hf isotopes were measured by LA-ICPMS at the Arizona LaserChron Center for representative zircons from all samples of metasedimentary and (meta)plutonic rocks analyzed in this study (Table 1; Appendix D).

Methods

Arizona LaserChron Center, University of Arizona

Traditional zircon extraction methods including jaw-crusher, pulverizer/disk mill, Gemini table, magnetic separation, and heavy liquid gravity separation were used to produce heavy mineral separates at the University of Iowa. A representative split of zircon was mounted onto a 1-inch (2.5 cm) epoxy puck, along with multiple fragments of U-Pb reference materials SL (564 ± 4 Ma; Gehrels et al. 2008), R33 (420.5 ± 0.2 Ma, Mattinson 2010) and FC (1099 ± 1 Ma, Paces and Miller 1993) and Hafnium standards (R33, SL, FC, Plesovice, Temora, Mud Tank, and 91500; Woodhead and Hergt 2005; Blichert-Toft 2008; Sláma et al. 2008; Bahlburg et al. 2010). The mounts were hand polished with sandpaper to expose the core of the unknown grains. Mounts were then mechanically diamond-polished to 1 µm and carbon-coated. Cathodoluminescence (CL) images for each sample were made using a Hitachi S-3400N scanning electron microscope (SEM) at the University of Iowa MATFab facility. The carbon-coat was removed with 3 µm diamond polish and the mounts were washed in an ultrasonic bath of 1% HNO_3 and 1% HCl to remove surficial common Pb.

Table 1. *Summary of geochronological results for samples from the Klondike region analyzed in this study.*

Sample	Map unit	Lithology[1]	Latitude	Longitude	LA-ICPMS					CA-TIMS		
					N[2]	n[3]	Hf(n)	YPP[4] (Ma)	TuffZirc[5] (Ma)	n	$^{206}Pb/^{238}U$ (Ma)	±
Permian igneous rocks												
19MC-011	PJCg	Bt Granite (Jim Creek pluton)	63.807615	-139.604731	35	–	10	260	260.83 +1.19/ -2.48	6	260.84	0.07
19MC-015	PJCg	Two-mica granite (dike)	63.825469	-139.553986	36	–	10	263	263.68 +3.86/ -3.91	6	260.91	0.07
19MC-020	PSCg	Foliated metagranite (Sulphur Creek)	63.868467	-139.498816	29	–	9	250	249.50 +2.27/ -2.48	7	260.96	0.07
Klondike Schist - detrital zircon samples												
19MC-016	Psqm	Quartzite	63.960018	-139.345309	582	475	18	273	272.62 +0.34/ -0.87	_	_	_
19MC-017	Psa	Qtz-Fp schist	63.950575	-139.336909	477	341	19	248 (264)[6]	263.69 +0.60/ -0.45	12	262.25	0.06
20MC-003	Psa	Qtz-Pl-Ms schist	63.949031	-139.339039	226	67	15	262	262.38 +0.77/ -0.86	_	_	_
19MC-018	Psa/Psqm	Ms-Qtz-Pl-Chl schist	63.895336	-139.318573	520	338	26	262 (270)[6]	270.74 +0.33/ -0.44	_	_	_
19MC-021	Psq	Qtz-Ms schist	63.916888	-139.259005	595	487	21	262	262.07 +0.42/ -0.21	3	261.51	0.11

Notes: 1) mineral abbreviations after Kretz (1983); 2) total number of zircon analyzed; 3) number of "acceptable dates"; 4) YPP = youngest graphical peak; 5) TuffZirc age calculated using Isoplot 4.15 (Ludwig, 2008; Ludwig & Mundil, 2002); 6) age in bracket corresponds to prominent peak in that sample, Fig. 8.

LA-ICPMS U-Pb analysis

U-Pb isotopic analyses were conducted at the ALC using a laser ablation mutlicollector inductively coupled plasma mass spectrometer (LA-MC-ICPMS) Nu instrument. Cathodoluminescence images were used to avoid inclusions and to guide spot location in uniform crystal domains. Samples were analyzed using a Photonmachines Analyte G2 excimer laser (l = 193 nm) coupled with the hyper-Nu method of Sundell et al. (2020) with a 30 µm spot size for n = 300 and n = 600.

Data reduction was performed with AgeCalcML for the hyper-Nu (Sundell et al., 2020). $^{206}Pb/^{238}U$ dates are used for apparent ages less than 900 Ma, whereas $^{207}Pb/^{206}Pb$ ages are used for analyses older than 900 Ma. Data was filtered to exclude: 1) analyses with >10% discordance, >5% reverse discordance based on [($^{206}Pb/^{238}U$ date / $^{206}Pb/^{207}Pb$ date) – analytical error propagated at 2σ level] following equations in Gibson et al. (2021); 2) >10% 2σ analytical uncertainty of the $^{206}Pb/^{238}U$ date; and 3) >50% uncertainty of the $^{207}Pb/^{206}Pb$ date. The U-Pb data are presented in Appendix A.

LA-ICPMS Hf analysis

Representative concordant zircon from each age population were analyzed for Hf isotope composition by LA-MC-ICP-MS using the methods of Cecil et al. (2011) and Gehrels and Pecha (2014). A spot size of 40 µm was used and placed directly on top of U-Pb analysis pits. The Hf isotopic data are plotted on Hf evolution diagrams with initial $^{176}Hf/^{177}Hf$ ratios expressed in

εHf_t notation indicating the Hf isotopic composition at the time of zircon crystallization relative to the chondritic uniform reservoir (CHUR; Bouvier et al., 2008). The Hf isotopic data are presented in Appendix D.

Isotope Geology Laboratory, Boise State University

LA-ICPMS U-Pb analysis

Zircon grains were separated from rocks using standard techniques, annealed at 900°C for 60 hours in a muffle furnace, and mounted in epoxy and polished until their centres were exposed. Cathodoluminescence images were obtained with a JEOL JSM-300 scanning electron microscope and Gatan MiniCL. Zircon was analyzed by LA-ICPMS using a ThermoElectron X-Series II quadrupole ICPMS and New Wave Research UP-213 Nd:YAG UV (213 nm) laser ablation system. In-house analytical protocols, standard materials, and data reduction software were used for acquisition and calibration of U-Pb dates and a suite of high field strength elements (HFSE) and rare earth elements (REE). Zircon was ablated with a laser spot of 25 µm wide using fluence and pulse rates of 5 J/cm^2 and 5 Hz, respectively, during a 45 second analysis (15 second gas blank, 30 second ablation) that excavated a pit ~15 µm deep. Ablated material was carried by a 1.2 L/min He gas stream to the nebulizer flow of the plasma. Dwell times were 5 ms for Si and Zr, 200 ms for ^{49}Ti and ^{207}Pb, 80 ms for ^{206}Pb, 40 ms for ^{202}Hg, ^{204}Pb, ^{208}Pb, ^{232}Th, and ^{238}U and 10 ms for all other HFSE and REE. Background count rates for each analyte were obtained prior to each spot analysis and subtracted from the raw count rate for each analyte. Ablation pits that appear to have intersected glass or mineral inclusions were identified based on Ti and P. U-Pb dates from these analyses are considered valid if the U-Pb ratios appear to have been unaffected by the inclusions. Analyses that appear contaminated by common Pb were rejected based on mass 204 being above baseline. For concentration calculations, background-subtracted count rates for each analyte were internally normalized to ^{29}Si and calibrated with respect to NIST SRM-610 and -612 glasses as the primary standards. Temperature was calculated from the Ti-in-zircon thermometer (Watson et al., 2006). As there are no constraints on the activity of TiO_2, an average value in crustal rocks of 0.8 was used.

Data were collected in four experiments in November 2020. For U-Pb and ^{207}Pb/^{206}Pb dates, instrumental fractionation of the background-subtracted ratios was corrected, and dates were calibrated with respect to interspersed measurements of zircon standards and reference materials. The primary standard Plešovice zircon (Sláma et al., 2008) was used to monitor time-dependent instrumental fractionation based on two analyses for every 10 analyses of unknown zircon. A secondary correction to the ^{206}Pb/^{238}U dates was made based on results from the zircon standards Seiland (531 Ma, Kuiper et al., 2022) and Zirconia (327 Ma, unpublished data, Boise State University), which were treated as unknowns and measured once for every 10 analyses of unknown zircon. These results showed a linear age bias of several percent that is related to the ^{206}Pb count rate. The secondary correction is thought to mitigate matrix-dependent variations due to contrasting compositions and ablation characteristics between the Plešovice zircon and other standards (and unknowns).

Radiogenic isotope ratio and age error propagation for all analyses includes uncertainty contributions from counting statistics and background subtraction. The standard calibration uncertainty for U/Pb is the local standard deviation of the polynomial fit to the fractionation factor of Plešovice versus time and for ^{207}Pb/^{206}Pb is the standard error of the mean of the fractionation factor of Plešovice. These uncertainties for each experiment are shown in the footnotes of data tables in Appendix B. Age interpretations are based on ^{207}Pb/^{206}Pb dates for analyses with ^{207}Pb/^{206}Pb and ^{206}Pb/^{238}U dates >1500 Ma. Otherwise, interpretations are

based on $^{206}Pb/^{238}U$ dates. Analyses with discordance (based on comparison of $^{207}Pb/^{235}U$ and $^{206}Pb/^{238}U$ dates) >5% (including 2σ error on discordance) are not considered. Weighted mean $^{206}Pb/^{238}U$ dates are calculated from equivalent dates (probability of fit >0.05) using Isoplot 3.0 (Ludwig, 2008). Errors are 2σ.

CA-TIMS U-Pb analysis

U-Pb dates were obtained by the CA-TIMS method from analyses composed of single zircon grains (Table 1), modified after Mattinson (2005). Zircon was removed from the epoxy mounts for dating based on CL images and LA-ICPMS data.

Zircon was put into 3 ml Teflon PFA beakers and loaded into 300 µl Teflon PFA microcapsules. Fifteen microcapsules were placed in a large-capacity Parr vessel and the zircon partially dissolved in 120 µl of 29 M HF for 12 hours at 190°C. Zircon was returned to 3 ml Teflon PFA beakers, HF was removed, and zircon was immersed in 3.5 M HNO_3, ultrasonically cleaned for one hour, and fluxed on a hotplate at 80°C for one hour. The HNO_3 was removed and zircon was rinsed twice in ultrapure H_2O before being reloaded into the 300 µl Teflon PFA microcapsules (rinsed and fluxed in 6 M HCl during sonication and washing of the zircon) and spiked with the Boise State University mixed ^{233}U-^{235}U-^{205}Pb tracer solution (BSU-1B). Zircon was dissolved in Parr vessels in 120 µl of 29 M HF with a trace of 3.5 M HNO_3 at 220°C for 48 hours, dried to fluorides, and re-dissolved in 6 M HCl at 180°C overnight. U and Pb were separated from the zircon matrix using an HCl-based anion-exchange chromatographic procedure (Krogh, 1973), eluted together and dried with 2 µl of 0.05 N H_3PO_4.

Pb and U were loaded on a single outgassed Re filament in 5 µl of a silica-gel/phosphoric acid mixture (Gerstenberger and Haase, 1997), and U and Pb isotopic measurements made on a GV Isoprobe-T IsotopX mutlicollector thermal ionization mass spectrometer equipped with an ion-counting Daly detector. Pb isotopes were measured by peak-jumping all isotopes on the Daly detector for 160 cycles, and corrected for 0.16 ± 0.03%/a.m.u. (1σ) mass fractionation. Transitory isobaric interferences due to high-molecular weight organics, particularly on ^{204}Pb and ^{207}Pb, disappeared within approximately 60 cycles, while ionization efficiency averaged 10^4 cps/pg of each Pb isotope. Linearity (to ≥1.4 x 10^6 cps) and the associated deadtime correction of the Daly detector were determined by analysis of NBS982. Uranium was analyzed as UO_2^+ ions in static Faraday mode on 10^{12} ohm resistors for 300 cycles, and corrected for isobaric interference of $^{233}U^{18}O^{16}O$ on $^{235}U^{16}O^{16}O$ with an $^{18}O/^{16}O$ of 0.00206. Ionization efficiency averaged 20mV/ng of each U isotope. Uranium mass fractionation was corrected using the known $^{233}U/^{235}U$ ratio of the Boise State University tracer solution.

The U-Pb dates and uncertainties were calculated using the algorithms of Schmitz and Schoene (2007), calibration of BSU-1B tracer solution of $^{235}U/^{205}Pb$ of 77.93 and $^{233}U/^{235}U$ of 1.007066, $^{238}U/^{235}U$ of 137.818 (Hiess et al., 2012), and U decay constants recommended by Jaffey et al. (1971). $^{206}Pb/^{238}U$ ratios and dates were corrected for initial ^{230}Th disequilibrium using $D_{Th/U}$ = 0.20 ± 0.05 (1σ) and the algorithms of Crowley et al. (2007), resulting in an increase in the $^{206}Pb/^{238}U$ dates of ~0.09 Ma. All common Pb in analyses was attributed to laboratory blank and subtracted based on the measured laboratory Pb isotopic composition and associated uncertainty. U blanks are estimated at 0.013 pg. Weighted mean $^{206}Pb/^{238}U$ dates are calculated from equivalent dates (probability of fit >0.05) using Isoplot 3.0 (Ludwig, 2008). Errors are 2σ.

Results

Igneous zircons

Sample 19MC-011 is a coarse-grained biotite granite collected from the main body of the Jim Creek pluton (Figs. 2 and 4c). Although the granite at this locality shows little strain, the margin of the pluton locally exhibits deformation fabrics and intercalations with the host rocks (Fig. 4e). At locality 19MC-011 biotite occurs in clots along with epidote and garnet that define a weak foliation; the biotite is partially chloritized. A sample from this outcrop was previously dated at 252.4 ± 0.4 Ma by multi-grain isotope dilution thermal ionization mass spectrometry (ID-TIMS; Beranek and Mortensen, 2011). Thirty-five LA-ICPMS spots on zircon from sample 19MC-011 yielded $^{206}Pb/^{238}U$ dates between 269.0 ± 6.7 and 249.1 ± 5.3 Ma, and a weighted average of 260.3 ± 1.4 Ma (mean standard weighted deviation [MSWD] = 0.66, probability of fit [pof] = 0.93; Appendix B; Fig. 5a,b). Six zircons were analyzed by CA-TIMS and yielded $^{206}Pb/^{238}U$ dates between 260.92 ± 0.18 and 260.80 ± 0.18 Ma with a weighted average of 260.84 ± 0.07 Ma (MSWD = 0.4, pof = 0.86; Fig. 6a,b; Appendix C); this is interpreted as the crystallization age of the Jim Creek pluton. Epsilon Hf_t values for zircon in sample 19MC-011 range from -5.4 to -16.8 (Fig. 7a; Appendix D).

Sample 19MC-015 is from a granite dike east of the main body of the Jim Creek pluton. Beranek and Mortensen (2011) previously reported a $^{207}Pb/^{235}U$ monazite age of 252.5 ± 1.1 Ma from this dike. The dike is composed of coarse-grained, two-mica, garnet-bearing granite. The granite lacks apparent foliation and locally cuts foliated graphitic schist (Fig. 4d). In thin section, the granite shows evidence of recrystallization (Fig. 4f). Thirty-six LA-ICPMS spots on zircon from sample 19MC-015 yielded $^{206}Pb/^{238}U$ dates between 275.1 ± 8.9 and 250.7 ± 7.7 Ma with a weighted average of 264.7 ± 1.9 Ma (MSWD = 1.5, pof = 0.05; Appendix B; Fig. 5c,d). Six zircons were selected for CA-TIMS and yielded $^{206}Pb/^{238}U$ dates between 261.09 ± 0.18 and 260.83 ± 0.18 Ma and a weighted average of 260.91 ± 0.07 Ma (MSWD = 1.1, pof = 0.34; Fig. 6c,d; Appendix C). This is interpreted as the crystallization age for this dike. Epsilon Hf_t values for zircon in sample 19MC-015 range from -4.5 to -9.1 (Fig. 7b; Appendix D).

Sample 19MC-020 is a strongly foliated quartz-feldspar augen metagranite of the Sulphur Creek orthogneiss collected in proximity of the Ninemile thrust (Figs. 2 and 4a,b; Table 1). The foliation is defined by quartz-feldspar-muscovite; biotite clots at high angle to the foliation are relic igneous phenocrysts. Beranek and Mortensen (2011) previously reported U-Pb dating results from a sample collected at this outcrop. Dating of multi-grain zircon fractions by ID-TIMS yielded a $^{206}Pb/^{238}U$ age of 259.9 ± 0.8 Ma from two concordant fractions; two other fractions show evidence for inherited cores and possible lead loss. LA-ICPMS analyses from the same sample yielded a weighted average $^{206}Pb/^{238}U$ age of 259.0 ± 0.8 Ma (Beranek and Mortensen, 2011). Twenty-nine LA-ICPMS spots on zircon from sample 19MC-020 yielded $^{206}Pb/^{238}U$ dates between 262.0 ± 6.3 and 240.0 ± 9.0 Ma and a weighted average of 249.1 ± 1.8 Ma (MSWD = 0.91, pof = 0.58; Appendix B; Fig. 5e,f). Seven zircons from this sample were analyzed by CA-TIMS and yielded $^{206}Pb/^{238}U$ dates between 261.07 ± 0.17 and 260.86 ± 0.18 Ma and a weighted average of 260.96 ± 0.07 Ma (MSWD = 0.8, pof = 0.59; Fig. 6e,f; Appendix C) that is interpreted as the crystallization age of the Sulphur Creek orthogneiss. Epsilon Hf_t values for zircon in sample 19MC-020 range from -8.8 to -17.5 (Fig. 7c; Appendix D).

Detrital zircons

Five samples of metaclastic rocks were collected from various map units of the Klondike Schist (Fig. 2; Table 1). Sample 19MC-016 is a quartzite from unit Psqm of Mortensen (1996) collected along the Bonanza Creek road (Fig. 2). The quartzite is massive, tan weathering and preserves well-rounded quartz grains (Fig. 3d). A felsic schist from unit Psqm has an interpreted age of 263 ± 4 Ma based on discordant ID-TIMS analyses of multi-grain zircon fractions (Mortensen, 1990). Sample 19MC-016 yielded 475 acceptable dates from a total of

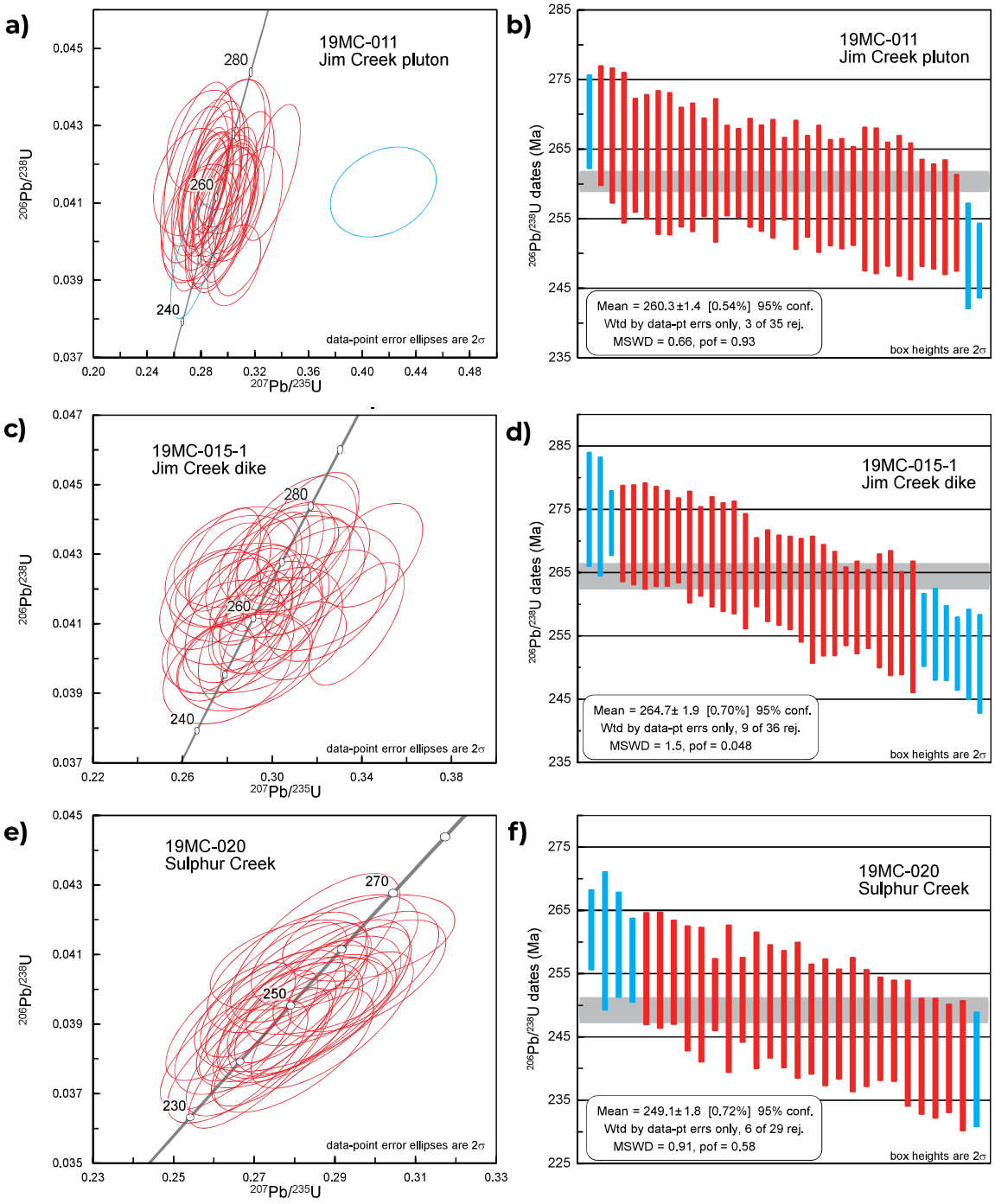

Figure 5. *Concordia diagrams and ranked plots of $^{206}Pb/^{238}U$ dates for igneous zircons analyzed by LA-ICPMS at Boise State University (Appendix B). Red bars indicate dates used in weighted mean calculation.*

582 analyses with 99% of dates ranging from 367 to 237 Ma and defining a peak at 273 Ma (TuffZirc age of 272.62 +0.34/ -0.87 Ma; Fig. 8a; Appendix A). Five zircons yielded Precambrian ages of 2788, 2522, 1738, 1014 and 655 Ma. Epsilon Hf_t values for Paleozoic zircon in sample 19MC-016 range from -1.2 to -14.4 (Fig. 9a; Appendix D). Two Precambrian grains have εHf_t values of -0.5 and -2.2.

Sample 19MC-017 is a quartzo-feldspathic schist from unit Psa of Mortensen (1996) collected along the east side of Bonanza Creek (Figs. 2 and 3b; Table 1). Mortensen (1990) reported an ID-TIMS U-Pb age of 261 ± 4 Ma for multi-grain zircon fractions from a moderately foliated

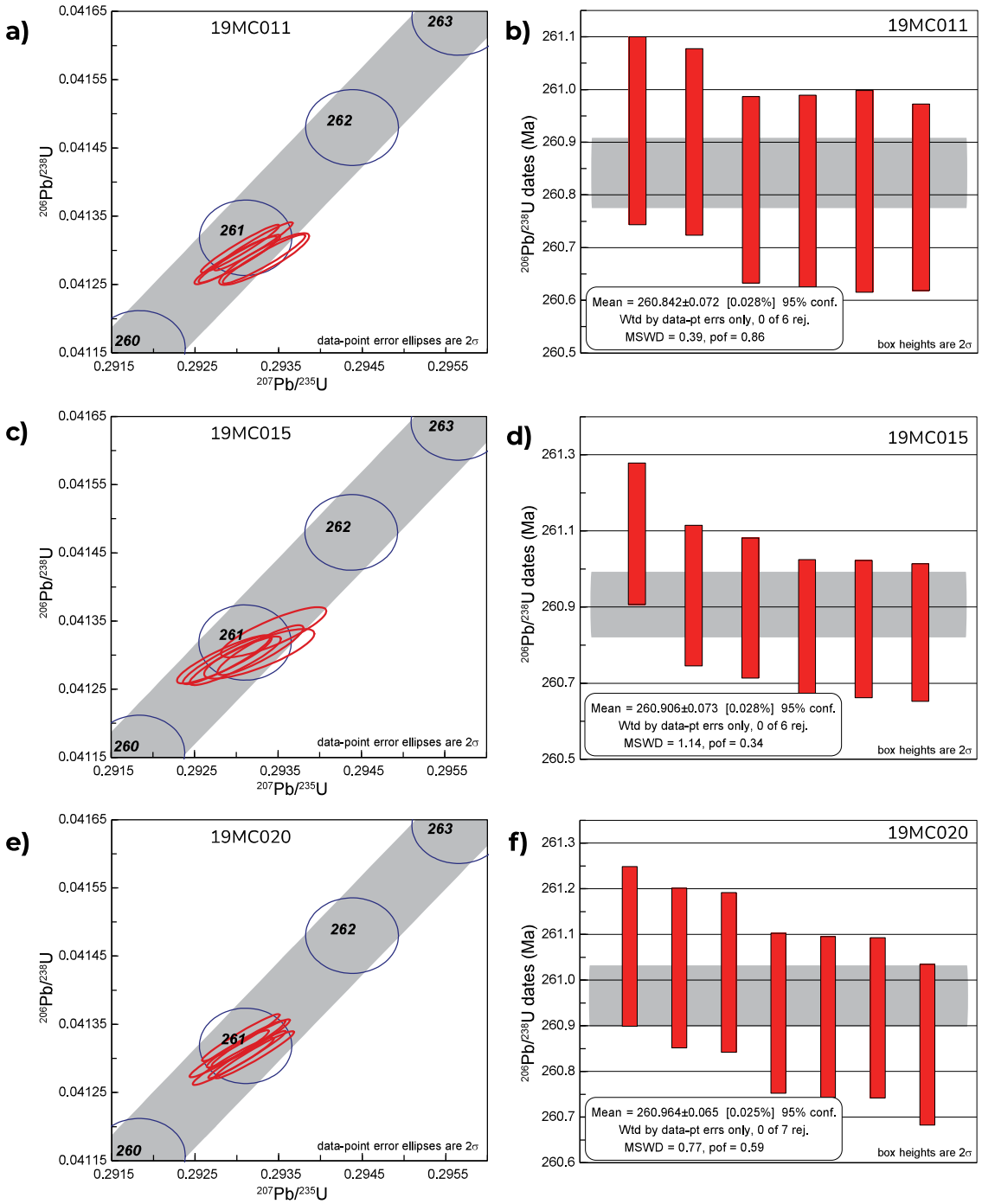

Figure 6. *Concordia diagrams and ranked plots of $^{206}Pb/^{238}U$ dates for igneous zircons analyzed by CA-TIMS at Boise State University (Appendix C).*

quartz-feldspar metaporphyry intruding unit Psa. The sample yielded 341 acceptable analyses from a total of 477 analyses with age peaks at 264 and 248 Ma (Fig. 5b; Appendix A). The youngest age peak is supported by ~27% of acceptable analyses and taken at face value would suggest an Early Triassic MDA for unit Psa of the Klondike Schist, an interpretation that is at odds with the ca. 261 Ma igneous age reported from this unit (Mortensen, 1990). To test these results, 12 zircons were selected across the range of dates obtained by LA-ICPMS and further analyzed using the CA-TIMS method (Appendix C). All 12 grains yielded overlapping $^{206}Pb/^{238}U$ dates between 262.35 ± 0.19 and 262.14 ± 0.18 Ma and a weighted average of 262.25 ± 0.06 Ma (MSWD = 0.5, pof = 0.88; Fig. 10a,b) that provides a robust MDA for unit

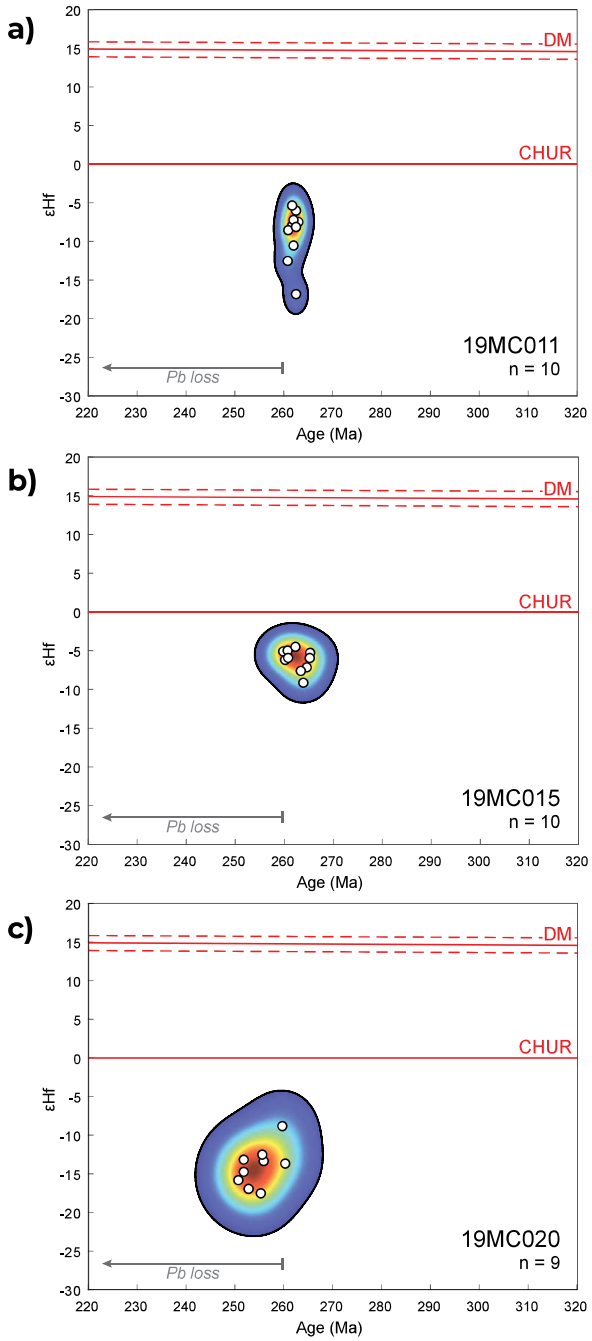

Figure 7. *Plots of εHf_t vs. age for representative igneous zircons from the Klondike region (data in Appendix D). Colour intensity contours within the 95th percentile envelope were plotted using HafniumPlotter of Sundell et al. (2019). LA-ICPMS dates younger than ca. 260 Ma are affected by Pb loss as discussed in Colpron et al. (2025). CHUR – chondritic uniform reservoir; DM – depleted mantle.*

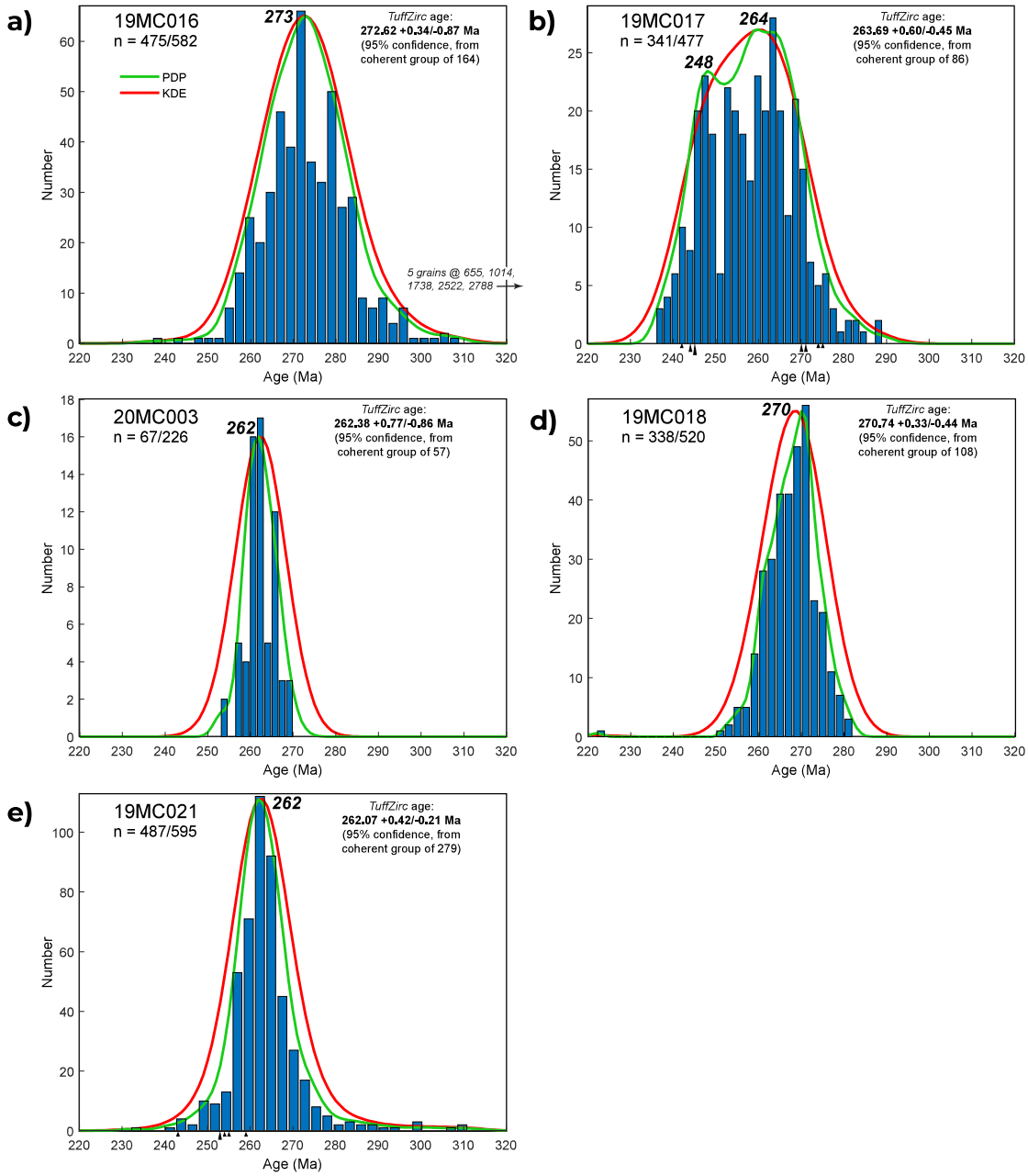

Figure 8. *Histograms, probability density plots (PDP) and kernel density estimates (KDE) for detrital zircon samples analyzed by LA-ICPMS at the Arizona LaserChron Center (data in Appendix A). Plots generated using AgeCalcML (Sundell et al., 2020). TuffZirc ages calculated using IsoPlot 4.15 (Ludwig, 2008; Ludwig and Mundil, 2002).*

Psa of the Klondike Schist. These results clearly indicate that sample 19MC-017 was subjected to significant Pb-loss that could not be detected by LA-ICPMS analyses. Epsilon Hf_t values for zircon in sample 19MC-017 range from -0.2 to -14.7 (Fig. 9b; Appendix D).

Another sample of metaclastic rock from unit Psa was collected on the west side of Bonanza Creek (20MC-003, Table 1), approximately 200 m southwest of locality 19MC-017 (Figs. 2 and 3c). Sample 20MC-003 yielded 67 acceptable dates out of 226 analyses that define a unimodal peak at 262 Ma (Fig. 8c; Appendix A; TuffZirc age = 262.38 +0.77/ -0.86 Ma) consistent with the MDA determined by CA-TIMS for 19MC-017. Epsilon Hf_t values for zircon in sample 20MC-003 range from -1.5 to -10.1 (Fig. 9c; Appendix D).

Sample 19MC-018 is a muscovite-plagioclase-quartz-garnet-chlorite schist collected at the contact between units Psa and Psqm along French Gulch (Fig. 2; Table 1). The rock is strongly foliated with coarse quartz porphyroclasts that probably represent deformed pebbles in a metawacke (Fig. 3e). It yielded 338 acceptable analyses from a total of 520 with a dominant peak at 270 Ma (Fig. 8d; Appendix A). Epsilon Hf_t values for zircon in sample 19MC-018 range from -3.0 to -10.8 (Fig. 9d; Appendix D).

Sample 19MC-021 is a quartz-mica schist from unit Psq, the structurally lowest unit in the Klondike Schist (Mortensen, 1996), collected along upper Bonanza Creek (Figs. 2 and 3f; Table 1). It yielded 487 acceptable dates from a total of 595 analyses with a unimodal peak at

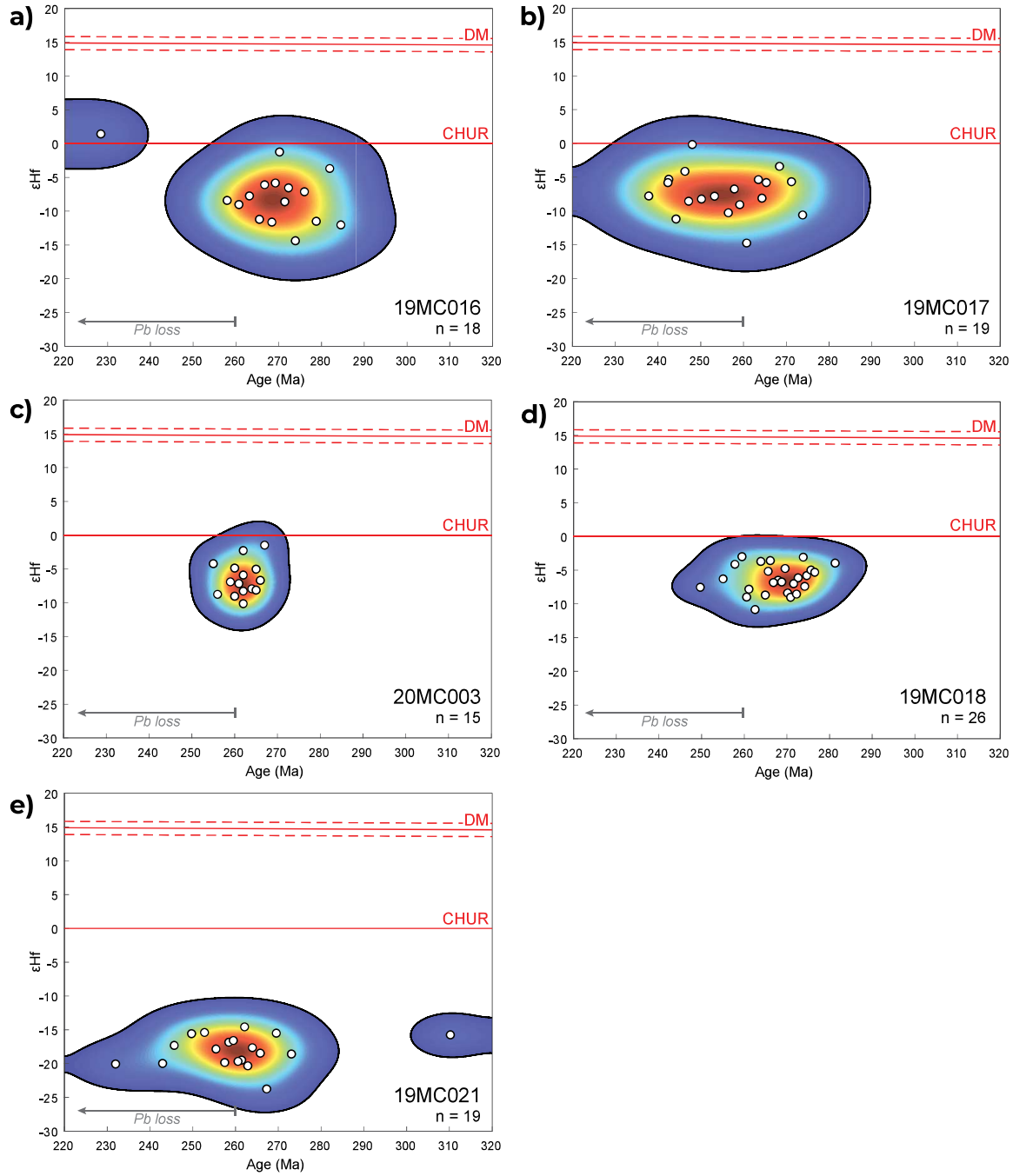

Figure 9. *Plots of εHf_t vs. age for representative detrital zircons from the Klondike region (data in Appendix D). Colour intensity contours within the 95th percentile envelope were plotted using HafniumPlotter of Sundell et al. (2019). LA-ICPMS dates younger than ca. 260 Ma are affected by Pb loss as discussed in Colpron et al. (2025). CHUR – chondritic uniform reservoir; DM – depleted mantle.*

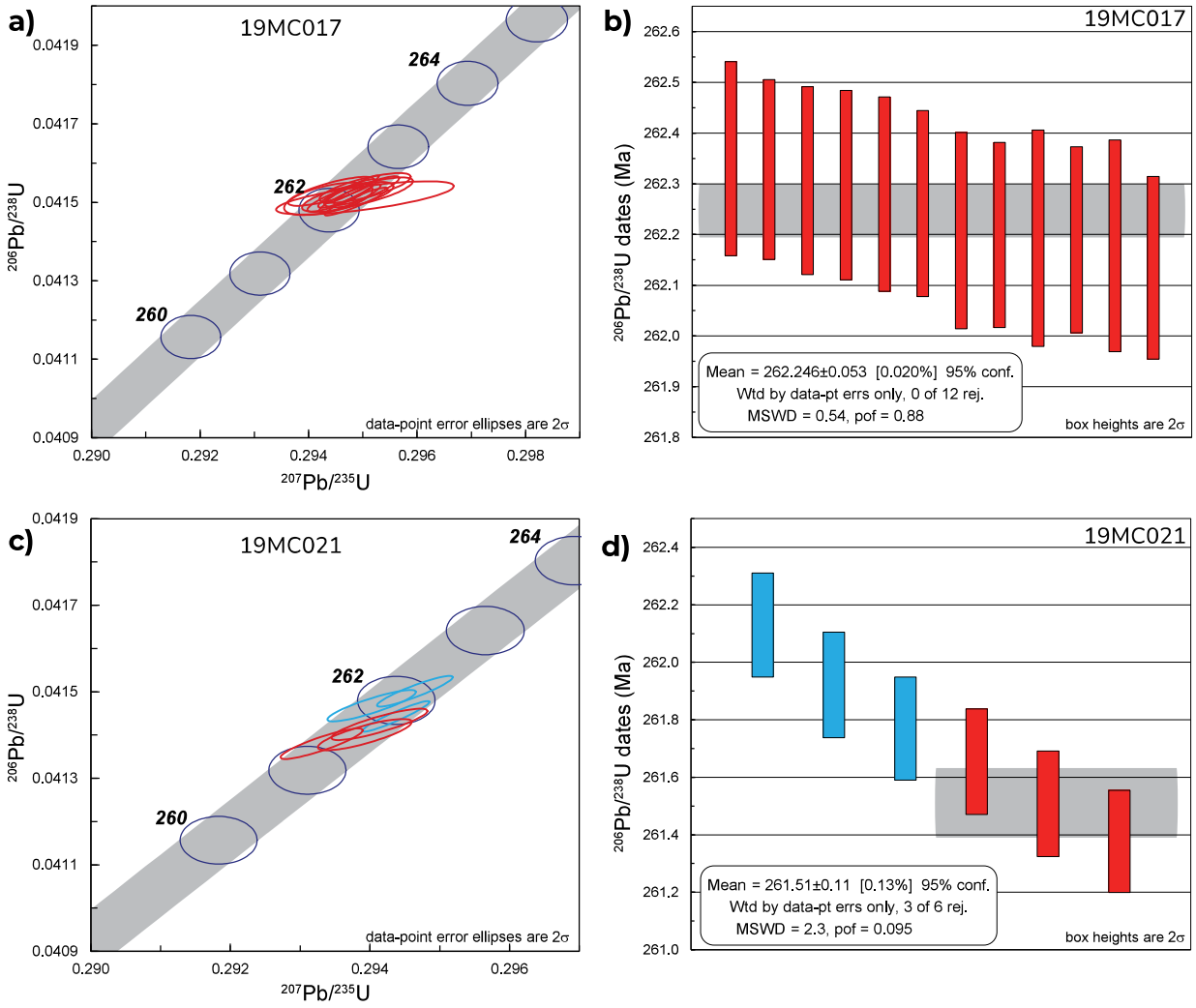

Figure 10. *Concordia diagrams and ranked plots of $^{206}Pb/^{238}U$ dates for detrital zircons analyzed by CA-TIMS at Boise State University (Appendix C). Red bars indicate dates used in weighted mean calculation.*

262 Ma (Fig. 8e; Appendix A). Six zircon grains were selected for CA-TIMS analysis to precisely establish the MDA for unit Psq. They yielded $^{206}Pb/^{238}U$ dates ranging from 261.38 ± 0.18 to 262.13 ± 0.18 Ma (Appendix C). The youngest three dates have a weighted average $^{206}Pb/^{238}U$ date of 261.51 ± 0.11 Ma (MSWD = 2.3, pof = 0.10; Fig. 10c,d). Epsilon Hf_t values for zircon in sample 19MC-021 range from -14.6 to -23.8 (Fig. 9e; Appendix D).

$^{40}Ar/^{39}Ar$ thermochronology

Mica from four samples of Jim Creek and Sulphur Creek plutons (Fig. 11) were analyzed in five aliquots using the $^{40}Ar/^{39}Ar$ step-heating method at the University of Manitoba (Appendix E) to determine the cooling ages of Permian intrusions in the region.

Methods

$^{40}Ar/^{39}Ar$ analysis – University of Manitoba

$^{40}Ar/^{39}Ar$ analytical work was performed at the University of Manitoba using a mutlicollector

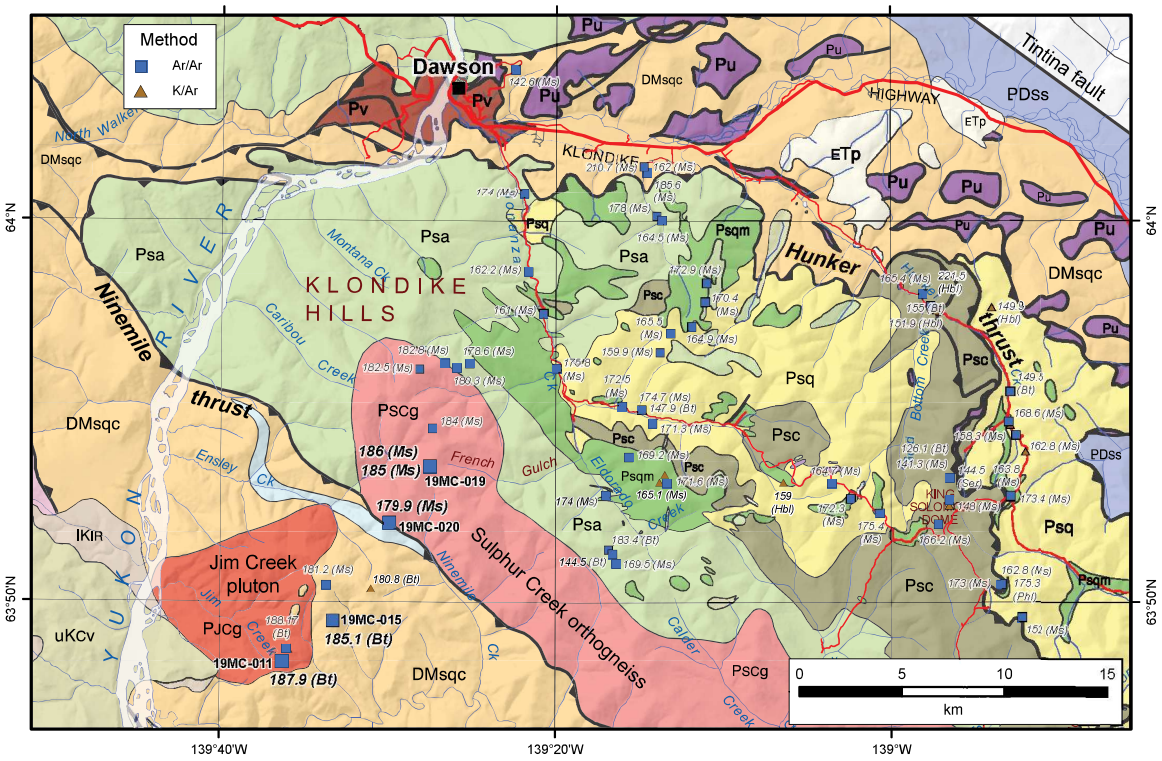

Figure 11. *Geological map of the Klondike region showing $^{40}Ar/^{39}Ar$ and K/Ar cooling ages. Larger symbols and bold types indicate samples analyzed for this study (Appendix E; Fig. 12); all other data are from Yukon Geological Survey (2023b, and references therein). See Figure 2 for map legend.*

Thermo Fisher Scientific ARGUSVI mass spectrometer, linked to a stainless steel Thermo Fisher Scientific extraction/purification line and Photon Machines (55 W) Fusions 10.6 CO_2 laser. Argon isotopes were measured using the following configuration: ^{40}Ar (H1; 1 x 10^{12} Ω resistor), ^{39}Ar (AX; 1 x 10^{13} Ω resistor), ^{38}Ar (L1; 1 x 10^{13} Ω resistor), ^{37}Ar (L2; 1 x 10^{13} Ω resistor) and ^{36}Ar (compact discrete dynode [CDD]). The sensitivity for argon measurements is ~6.3 x 10^{17} moles/fA as determined from measured aliquots of Fish Canyon Sanidine (Dazé et al., 2003; Kuiper et al., 2008).

Standards and unknowns were placed in 2 mm deep wells in 18 mm diameter aluminum disks, with standards placed strategically so that the lateral neutron flux gradients across the disk could be evaluated. Planar regressions were fit to the standard data, and the $^{40}Ar/^{39}Ar$ neutron fluence parameter, J, interpolated for the unknowns. All specimens were irradiated in the Cadmium-lined, in-core CLICIT facility of the Oregon State University TRIGA reactor. The duration of irradiation was 35 hours and the Fish Canyon sanidine (28.201 Ma; Kuiper et al., 2008) was used as monitor.

Irradiated samples were placed in a Cu sample tray, with a KBr cover slip, in a stainless-steel high vacuum extraction line and baked with an infrared lamp for 24 hours. Single crystals were either fused or step-heated using the laser for 1 minute and reactive gases were removed after ~3 minutes by a JANIS cryocooler at ~ -120°C, a NP-10 SAES getter at room temperature and a GP50 getter (C50 ST101 alloy) at 450°C prior to being admitted to an ARGUSVI mass spectrometer by expansion. Five argon isotopes were measured simultaneously over a period of 6 minutes. Measured isotope abundances were corrected for extraction-line blanks, which were determined before every sample analysis.

Detector intercalibration (IC) between the different faraday cups was monitored (in Qtegra)

every three days by peak hopping ^{40}Ar. The intercalibration factor between H1 and the CDD was measured with the unknowns by online analysis of air pipettes (IC values can be found in Appendix E). A value of 295.5 was used for the atmospheric $^{40}Ar/^{36}Ar$ ratio (Steiger and Jaëger, 1977) for the purposes of routine measurement of mass spectrometer discrimination using air aliquots, and correction for atmospheric argon in the $^{40}Ar/^{39}Ar$ age calculation. Corrections are made for neutron-induced ^{40}Ar from potassium, ^{39}Ar and ^{36}Ar from calcium, and ^{36}Ar from chlorine (Roddick, 1983; Renne et al., 1998; Renne and Norman, 2001). Data collection and reduction was performed using Pychron (Ross, 2019). The decay constants used were those recommended by Min et al. (2000).

Results

Biotite from sample 19MC-011 (Jim Creek pluton) yielded a disturbed age spectrum with no defined plateau segment and an integrated age of 187.9 ± 0.1 Ma (Fig. 12a). The last 7 steps (F-L) define a pseudo-plateau with an age of 190.5 ± 0.4 Ma (MSWD = 1.5; Appendix E).

Biotite from sample 19MC-015 (Jim Creek dike) also yielded a disturbed age spectrum but the last 10 steps (C-L) define a relatively flat pseudo-plateau with an age of 185.1 ± 0.5 Ma (Fig. 12b). The integrated age for this biotite is 183.7 ± 0.2 Ma (Appendix E).

Two aliquots of muscovite from sample 19MC-019 (Sulphur Creek orthogneiss) yielded good plateau ages of 186.0 ± 0.3 and 185.0 ± 0.4 Ma, and integrated ages of 185.9 ± 0.3 and 185.0 ± 0.2 Ma (Appendix E; Fig. 12c,d). Muscovite from another sample of Sulphur Creek orthogneiss (19MC-020) yielded a disturbed age spectrum with a pseudo-plateau including 6 steps (E-I) with an age of 179.9 ± 1.4 Ma (Fig. 12e; Appendix E). The integrated age for this muscovite is 178.8 ± 0.6 Ma.

These results add to the extensive $^{40}Ar/^{39}Ar$ dataset for the Klondike region with mica ages ranging ca. 188–140 Ma and >80% of samples yielding Jurassic cooling ages (Yukon Geological Survey, 2023b, and sources cited therein). These results indicate that the whole Klondike region cooled below ~300-350°C in the Jurassic.

Whole rock geochemistry

Lithogeochemical data for Permian rocks from the Yukon-Tanana terrane were compiled from published and unpublished sources, including Milidragovic et al. (2016), Ryan et al. (2018) and van Staal et al. (2018) (see Appendix F). Previously unpublished data for the Klondike Schist (collected by S. Piercey and J. Mortensen, 2002), the Jim Creek pluton and Sulphur Creek orthogneiss (collected by M. Colpron, 2019) are also compiled in Appendix F. These data are all included in the Yukon Geological Survey's lithogeochemistry compilation (2023a). Analytical methods are included in the original sources (and summarized in Appendix F, and Yukon Geological Survey, 2023a) and involved solid source methods (e.g., X-ray fluorescence for major elements) or fusions and subsequent analysis by inductively coupled plasma emission spectroscopy (major and minor elements) and inductively coupled plasma mass spectrometry (trace elements). These types of analytical methods were critical for ensuring dissolution of resistant phases (e.g., zircon, monazite) as many elements sensitive to petrological processes (e.g., HFSE and REE) are hosted in these phases.

The data is presented in Appendix F and discussed below for each of the main Permian rock assemblages in the Yukon-Tanana terrane of western Yukon, including the Klondike Schist and Sulphur Creek plutonic suite (including the Jim Creek pluton). Data from the Dawson–Clinton Creek assemblage (van Staal et al., 2018) is also reviewed for comparison. Samples were

initially screened for alteration using the Ruks et al. (2006) and Large et al. (2001) diagrams (Fig. 13). In both diagrams, most rocks lie within least altered fields, however, given that a significant number of samples lie outside these fields, the data presentation and evaluation are focused on elements that are resistant to alteration and metamorphism and considered immobile, including the HFSE (Zr, Hf, Nb, Ta, Y, Sc), REE (La-Lu), Th, V, TiO_2, and Al_2O_3.

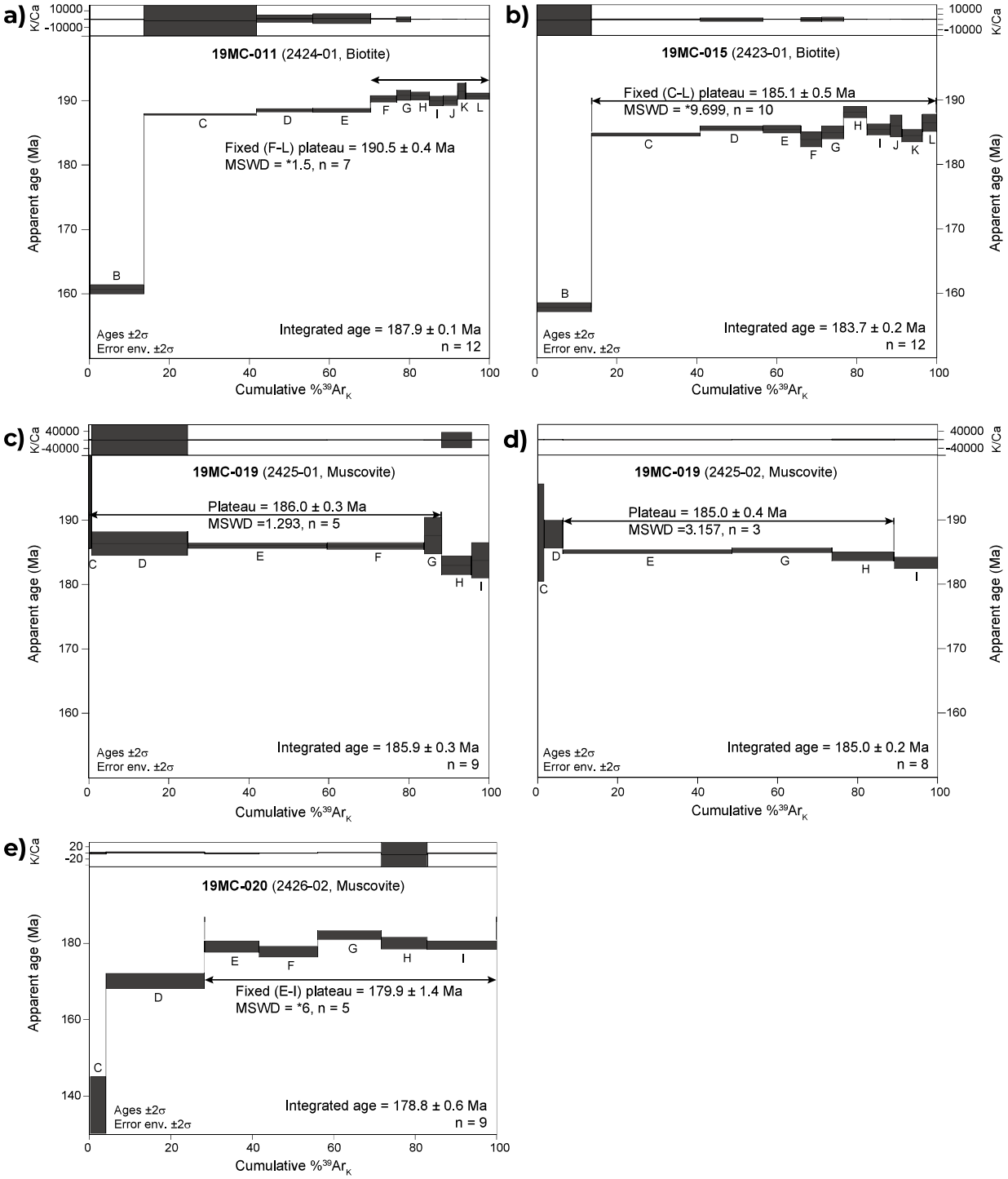

Figure 12. *$^{40}Ar/^{39}Ar$ age spectra for biotite and muscovite of the Jim Creek and Sulphur Creek plutons. Data is presented in Appendix E.*

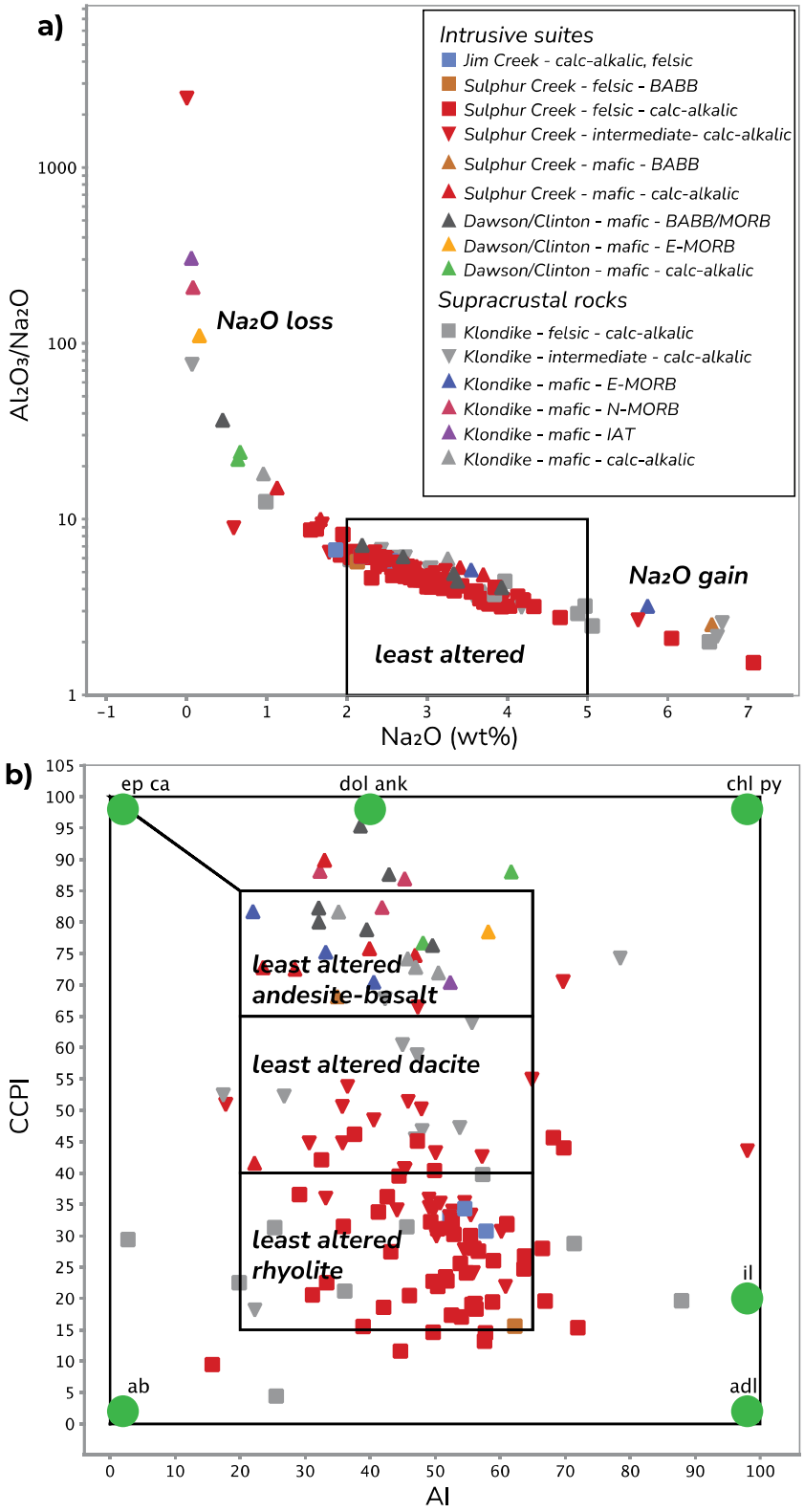

Figure 13. *Mobile element diagrams to evaluate degree of alteration in the Permian Yukon-Tanana terrane samples.* **a)** *Al_2O_3/Na_2O-Na_2O diagram of Ruks et al. (2006) based on the Spitz and Darling (1978) index. Most samples are unaltered, but a few have evidence for Na_2O loss and gains and are thus variably altered.* **b)** *Alteration box plot of Large et al. (2001) with the Hashimoto alteration index (AI) plotted against the chlorite-carbonate-pyrite index (CCPI). As in (a), most samples are unaltered, but some are altered; thus, limiting the use of major elements for petrological classification and determination of tectono-magmatic setting.*

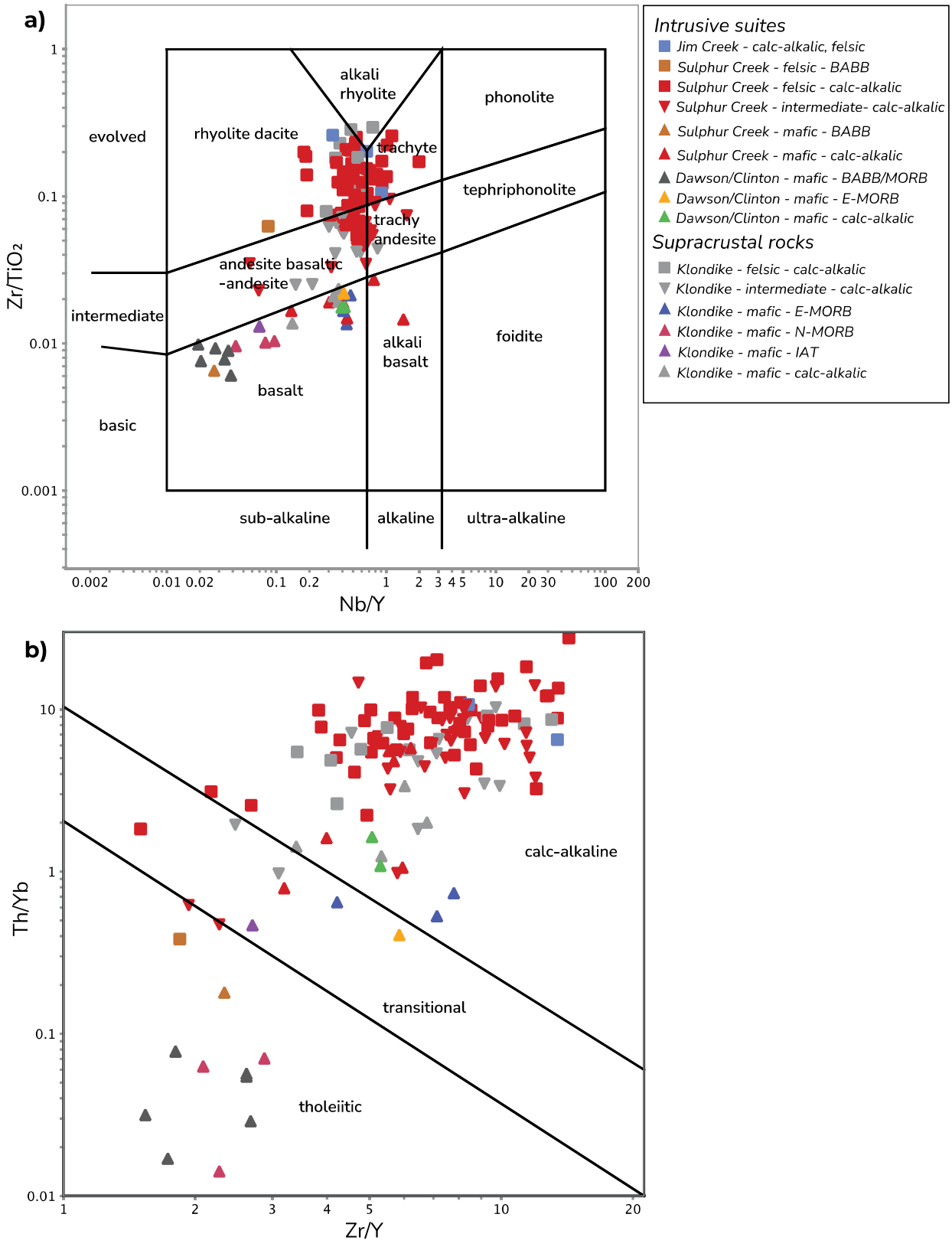

Figure 14. *Immobile element classification diagrams.* ***a)*** *Zr/TiO_2-Nb/Y diagram of Pearce (1996; modified from Winchester and Floyd, 1977).* ***b)*** *Th/Yb-Zr/Y diagram of Ross and Bedard (2009).*

Results

Klondike Schist

The Klondike Schist has mafic, intermediate, and felsic members. The mafic rocks have low Zr/TiO_2 but have variable Nb/Y, albeit all are subalkalic (Fig. 14). In Th/Yb-Zr/Y space one population of mafic rocks has tholeiitic affinities, one sample has a transitional affinity, another group overlaps the tholeiitic to weakly calc-alkalic fields, whereas another suite is predominantly within the calc-alkalic field, with two exceptions (Fig. 14). The different groups above exhibit different primitive mantle normalized multi-element patterns. Population 1 has flat patterns with light REE (LREE)-depletion like normal mid-ocean ridge basalt (N-MORB; Fig. 15a). In contrast, a second suite has higher LREE-enrichment and very weak negative Nb anomalies, consistent with enriched-MORB (E-MORB) affinities (Fig. 14b). Two suites have distinctive negative Nb anomalies, with one suite having flat heavy REE (HREE), weak

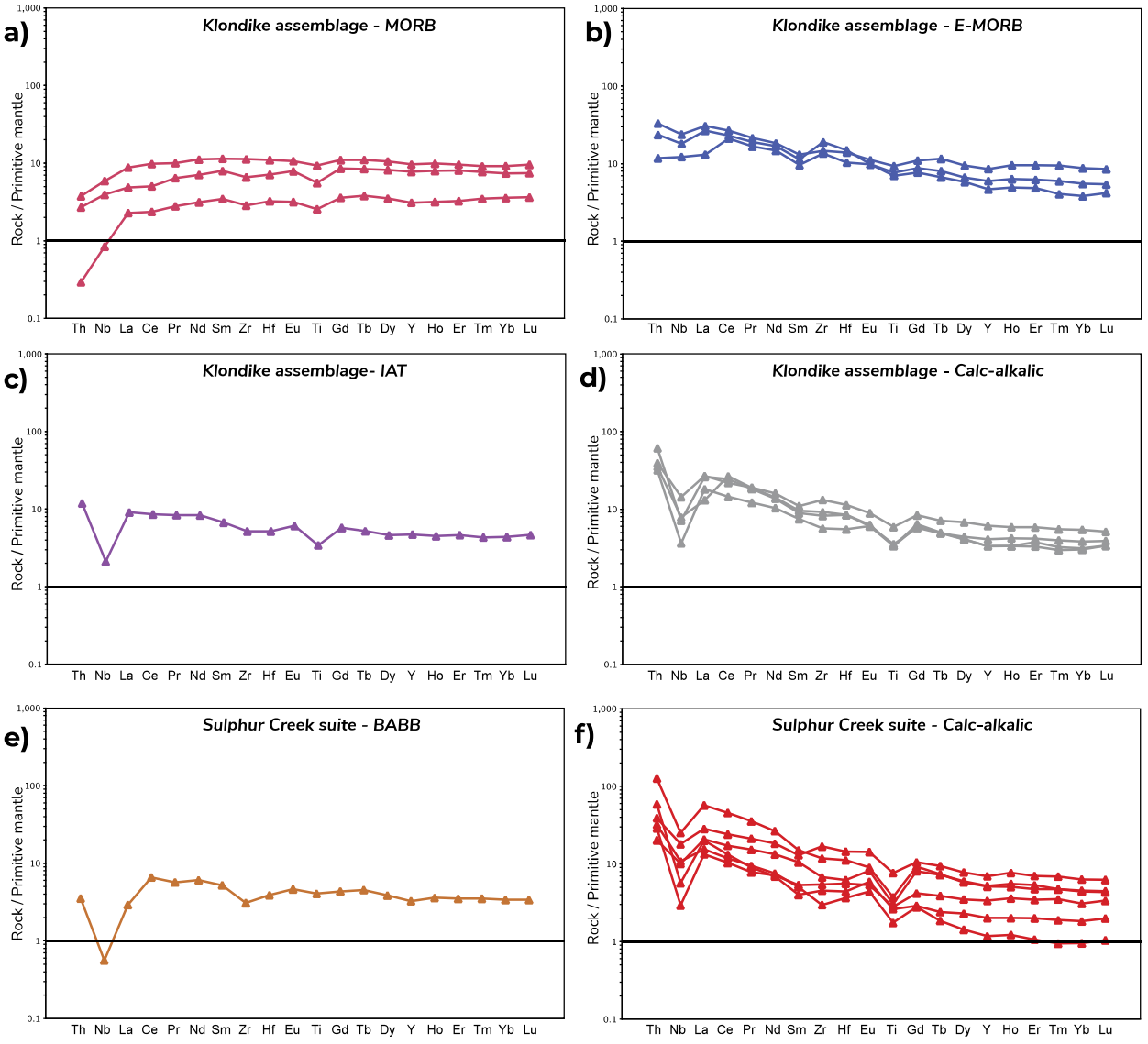

Figure 15. *Primitive mantle normalized multi-element plots for mafic rocks of the Klondike assemblage and Sulphur Creek plutonic suite. Primitive mantle values from Sun and McDonough (1989).* ***a)*** *Klondike assemblage – MORB affinity.* ***b)*** *Klondike assemblage – E-MORB affinity.* ***c)*** *Klondike assemblage – island arc tholeiite (IAT) affinity.* ***d)*** *Klondike assemblage – calc-alkalic affinity.* ***e)*** *Sulphur Creek suite – back-arc basin basalt affinity.* ***f)*** *Sulphur Creek suite – calc-alkalic affinity.*

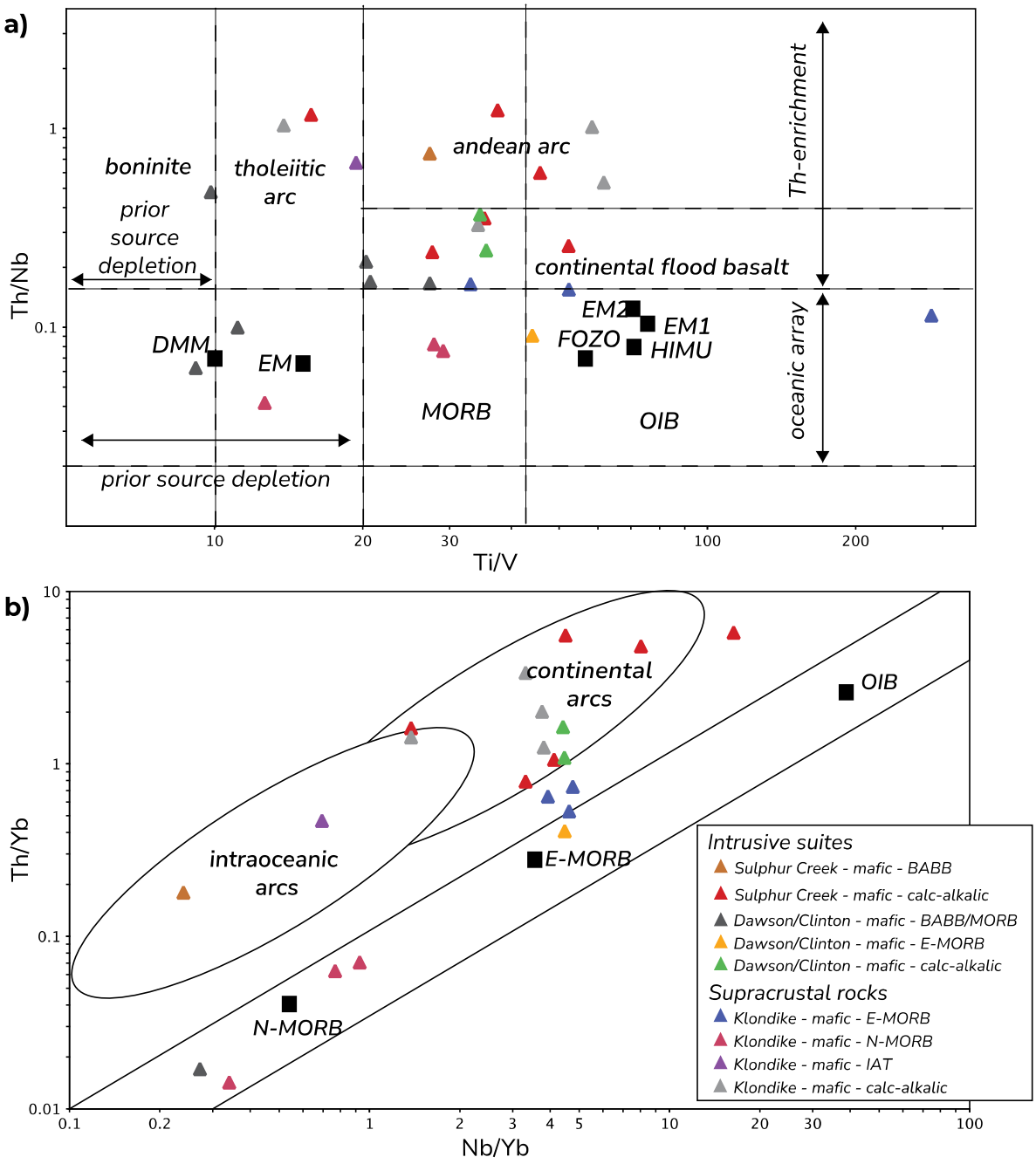

Figure 16. *Magma source and tectonic affinity diagrams for Mafic rocks. a) Th/Nb-Ti/V diagram of Shervais (2022). b) Th/Yb-Nb/Yb diagram of Pearce (2014), updated from Pearce and Peate (1995).*

LREE-enrichment, a minor negative Ti anomaly, and a distinctive negative Nb anomaly, typical of island arc tholeiitic rocks (Fig. 15c; Pearce et al., 1995; Pearce, 2014) and the second suite having negative Nb and Ti anomalies, but with greater LREE-enrichment, typical of calc-alkalic rocks (Fig. 15d; Pearce et al., 1995; Pearce, 2014). The N-MORB suite lies in the depleted mantle field in Th/Nb-Ti/V suite and near the N-MORB node on the Th/Yb-Nb/Yb diagram, whereas the E-MORB suite has intermediate but higher Ti/V and near the E-MORB node with higher Nb/Yb, but with higher Th/Yb and slight Th-enrichment (Fig. 16). The arc tholeiitic and calc-alkalic suites have intermediate to higher Ti/V and Th-enrichment and lie in the tholeiitic arc and Andean arc fields on the Th/Nb-Ti/V diagram, whereas on Th/Yb-Nb/Yb diagram these

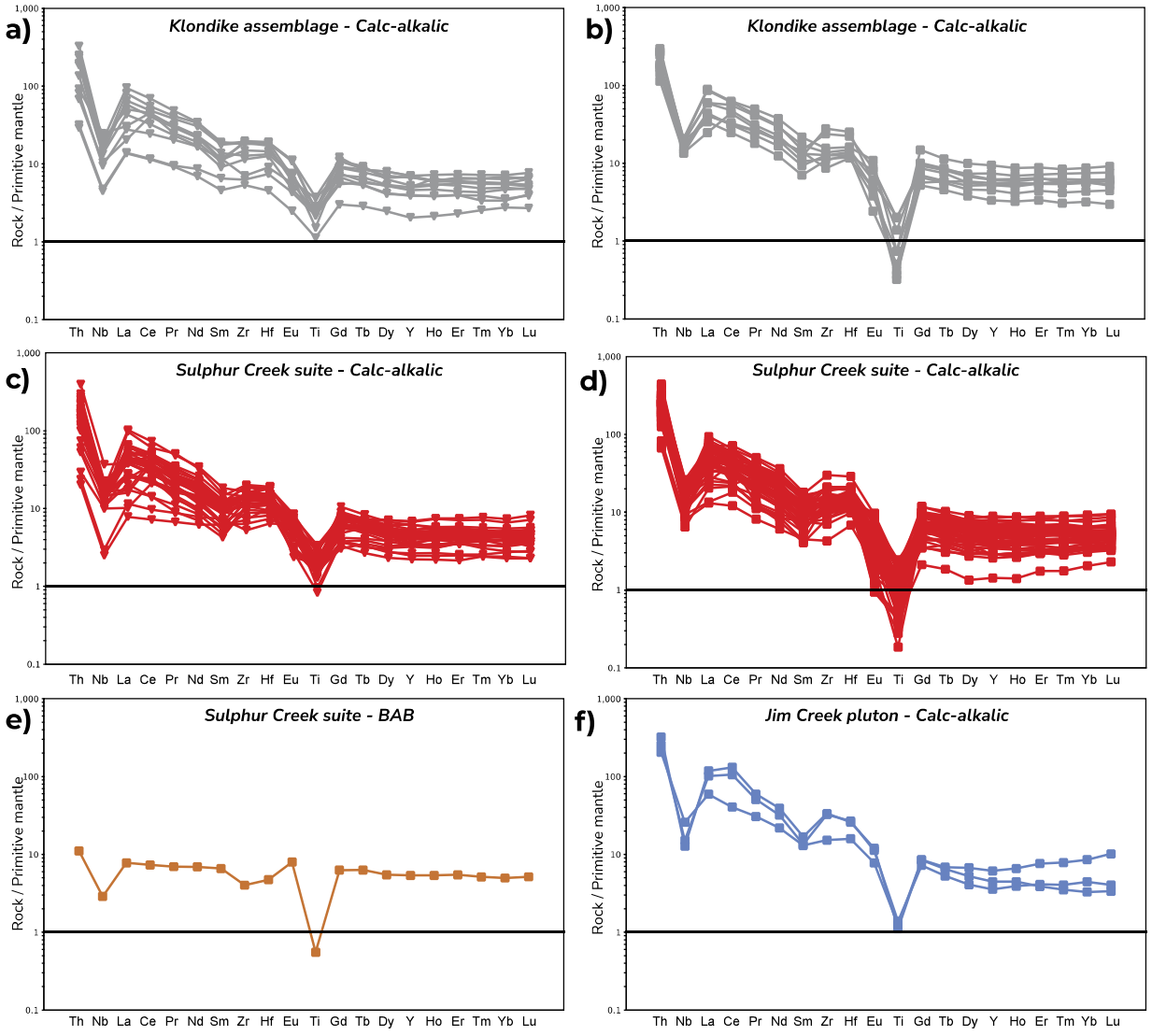

Figure 17. *Primitive mantle normalized multi-element plots for Permian intermediate and felsic rocks from the Yukon-Tanana terrane. Primitive mantle values from Sun and McDonough (1989).* ***a)*** *Klondike assemblage – intermediate – calc-alkalic affinity.* ***b)*** *Klondike assemblage – felsic – calc-alkalic affinity.* ***c)*** *Sulphur Creek suite – intermediate – calc-alkalic affinity.* ***d)*** *Sulphur Creek suite – felsic – calc-alkalic affinity.* ***e)*** *Sulphur Creek suite – felsic – back-arc basin affinity.* ***f)*** *Jim Creek pluton – felsic – calc-alkalic affinity.*

suites lie in the intra-oceanic and continental arc fields, respectively, consistent with derivation from depleted and weakly enriched mantle sources coupled with Th enrichment (Fig. 16).

The felsic and intermediate rocks of the Klondike Schist have intermediate to high Zr/TiO_2 and values that lie proximal to the Nb/Y boundary between alkalic and subalkalic rocks (Fig. 14). The vast majority of felsic to intermediate samples have calc-alkalic affinities, except for two intermediate samples that lie on the boundary of the transitional to calc-alkalic fields (Fig. 14). Both intermediate and felsic samples have LREE-enriched primitive mantle normalized multi-element signatures with very well-developed negative Nb and Ti anomalies and relatively flat HREE (Fig. 17a,b). Most felsic samples have Ga/Al-Zr systematics where the samples are in the I/S/M fields and a few outside in the A-type field, however, most samples have Nb-Y systematics consistent with I-type, volcanic arc affinities (Fig. 18).

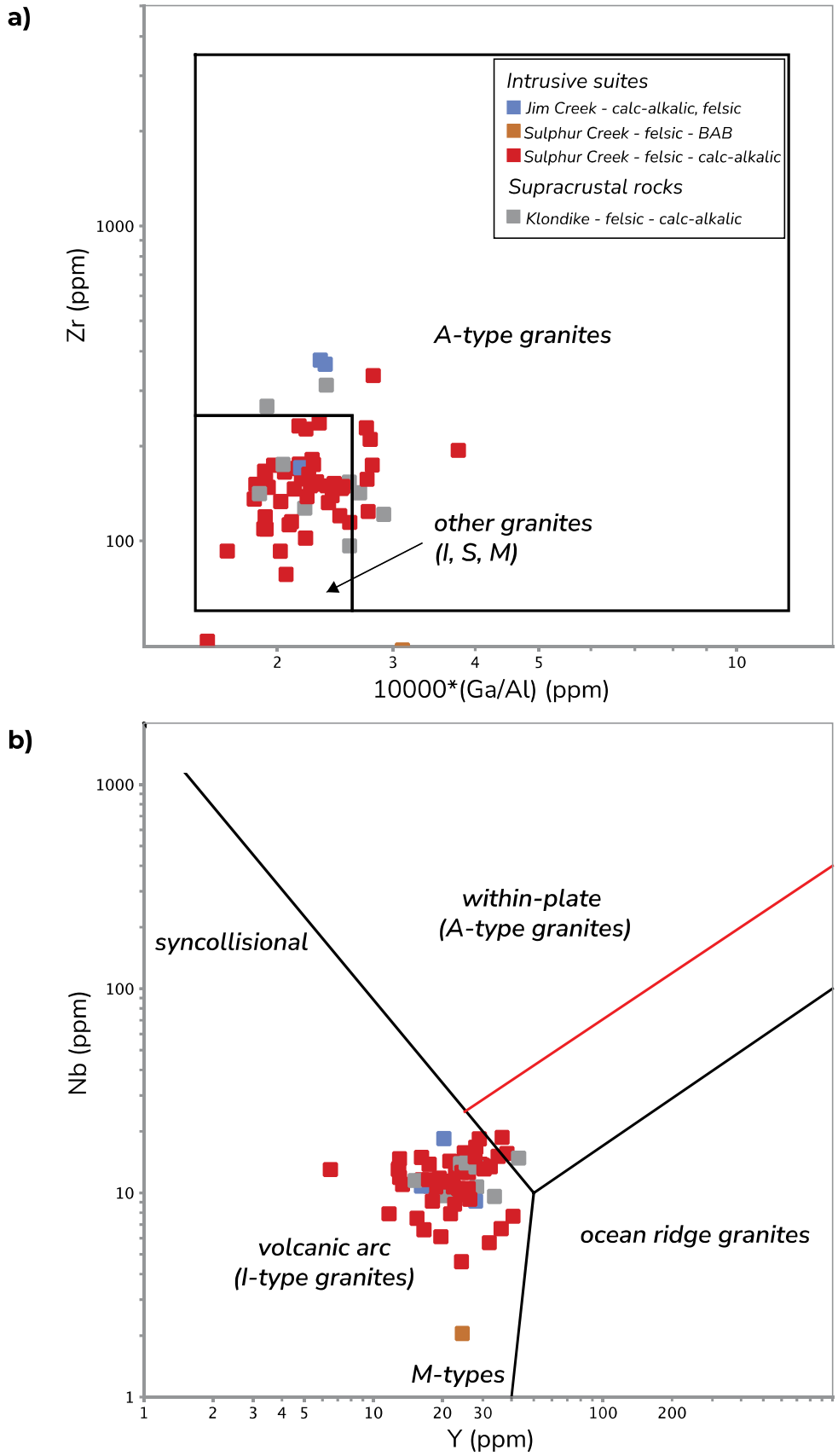

Figure 18. *Tectonic affinity diagrams for felsic rocks. a) Zr-Ga/Al plot of Whalen et al. (1987). b) Nb-Y diagram of Pearce et al. (1984).*

Sulphur Creek plutonic suite

The Sulphur Creek plutonic suite of intrusive rocks has mafic, intermediate, and felsic members. The mafic rocks have low Zr/TiO_2 and Nb/Y values that are subalkalic with two weakly alkalic samples (Fig. 14). One sample has a tholeiitic affinity, whereas the bulk of the samples have transitional to mostly calc-alkalic affinities in Th/Yb-Zr/Y space. The tholeiitic samples have flat primitive mantle normalized multi-element signatures with flat HREE and negative Nb anomalies (Fig. 15e), similar to island arc tholeiitic to back-arc basin rocks (e.g., Pearce et al., 1995; Pearce, 2014). The second suite has enrichments in LREE and negative Nb and Ti anomalies and flat to slightly depleted HREE (Fig. 15f), typical of calc-alkalic rocks (e.g., Pearce et al., 1995; Pearce, 2014). These two suites have divergent systematics in Th/Nb-Ti/V and Th/Yb-Nb/Yb space, where the tholeiitic samples come from depleted, N-MORB-like sources but with Th-enrichment, typical of 'arc' rocks, whereas the calc-alkalic suite has more enriched sources with higher Ti/V and Nb/Yb, typical of E-MORB, but with Th-enrichment common to continental arc environments (Fig. 16).

The felsic and intermediate rocks of the Sulphur Creek suite have intermediate to high Zr/TiO_2 and have Nb/Y ratios that are close to the alkalic- subalkalic boundary (Fig. 14). The vast majority of felsic to intermediate samples have calc-alkalic affinities, except for two intermediate samples that are transitional and one felsic sample that is tholeiitic (Fig. 14). Most intermediate to felsic samples also have LREE-enriched primitive mantle normalized multi-element signatures with strong negative Nb and Ti anomalies and relatively flat HREE (Fig. 17c,d). The tholeiitic sample has a flat pattern with a weak negative Th anomaly and a negative Ti anomaly, typical of felsic samples from back-arc environments and/or arc environments (Fig. 17e; Shukuno et al., 2006; Haraguchi et al., 2017). Most felsic samples have Ga/Al-Zr and Nb-Y systematics typical of I-type granites formed within continental arc environments with the exception of the tholeiitic sample, which has M-type features (Fig. 18), typical of rocks derived from melting of mafic crust (e.g., Shukuno et al., 2006; Haraguchi et al., 2017).

Jim Creek pluton

There are a limited number of samples from the Jim Creek pluton, but all have high Zr/TiO_2 and Nb/Y values that are on the subalkalic-alkalic boundary (Fig. 14). All samples have calc-alkalic affinities on the Th/Yb-Zr/Y diagram (Fig. 14b) and have LREE-enriched primitive mantle normalized multi-element patterns with flat to concave-upward HREE patterns, and negative Nb and Ti anomalies (Fig. 17f). The felsic samples have Ga/Al-Zr systematics with samples lying proximal to the I/S/M-type field and two samples with higher Zr values and within the A-type fields, however, in Nb-Y space all samples have volcanic arc/I-type affinities, typical of continental arc felsic rocks (Fig. 18).

Dawson–Clinton Creek assemblage

Rocks of the Dawson–Clinton Creek assemblage are mafic and subalkalic with low Nb/Y and Zr/TiO_2 values with most samples having tholeiitic affinities, one sample with transitional affinities, and two with calc-alkalic affinities (Fig. 14). These three different populations have distinctive primitive mantle normalized multi-element plots (Fig. 19). The tholeiitic suite has relatively flat patterns but with flat to weak negative Nb anomalies relative to Th and La, typical of N-MORB to back-arc basin basalt (BABB) rocks (Fig. 19a; Pearce and Stern, 2006). The transitional suite has similar patterns to the MORB/BABB suite and have flat HREE patterns, but with slight LREE-enrichment, typical of E-MORB (Fig. 19b; Sun and McDonough,

1989). The calc-alkalic suite has steeper patterns with LREE-enrichment, weakly developed negative Nb and Ti anomalies, albeit with less well-developed Nb and Ti anomalies compared to other calc-alkalic rocks in the Yukon-Tanana terrane (Fig. 19c; Piercey et al., 2006). The MORB/BABB suite have Th/Nb-Ti/V and Th/Yb-Nb/Yb systematics that are consistent with derivation from depleted mantle/N-MORB-type sources but with variable Th-enrichment (Fig. 16). In contrast, the E-MORB and calc-alkalic suite have higher Ti/V and Nb/Yb values consistent with derivation from weakly incompatible enriched sources, but with the calc-alkalic suite exhibiting Th-enrichment and plotting proximal to continental arc fields (Fig. 16).

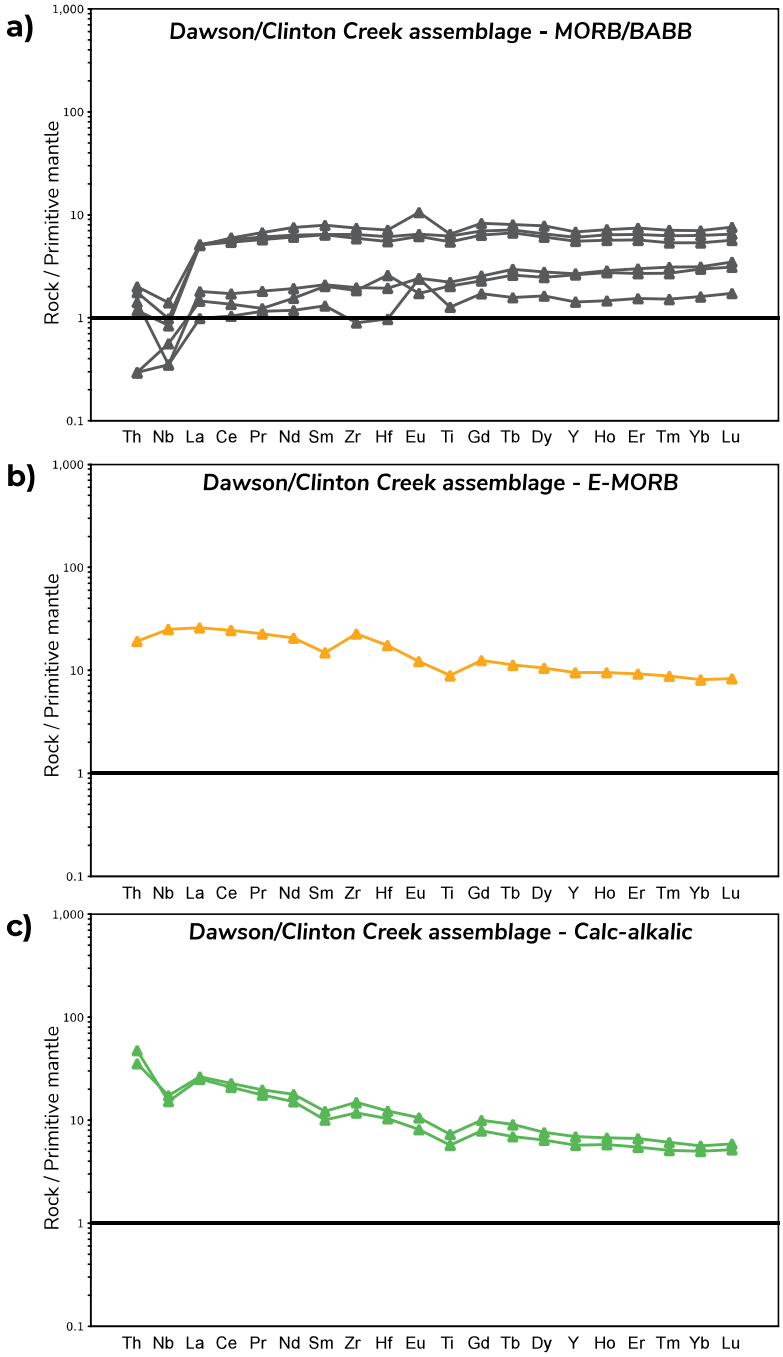

Figure 19. *Primitive mantle normalized multi-element plots for Permian mafic rocks from the Dawson–Clinton Creek assemblage. Primitive mantle values from Sun and McDonough (1989).* ***a)*** *Dawson–Clinton Creek assemblage – mid-ocean ridge basalt (MORB)/back-arc basin basalt affinity (BABB).* ***b)*** *Dawson–Clinton Creek assemblage – enriched mid-ocean ridge basalt (E-MORB) affinity.* ***c)*** *Dawson–Clinton Creek assemblage – calc-alkalic affinity.*

Summary

- Zircon from three samples of (meta)igneous rocks from the Jim Creek pluton and Sulphur Creek orthogneiss were dated using LA-ICPMS and CA-TIMS methods. All samples yielded equivalent $^{206}Pb/^{238}U$ dates of 260. 9 Ma (Fig. 6) thus eliminating the previously reported age difference between foliated Sulphur Creek orthogneiss (ca. 260 Ma) and undeformed Jim Creek pluton (ca. 252 Ma; Beranek and Mortensen, 2011).
- Detrital zircons from various units of the Klondike Schist generally yielded single age peaks indicating maximum depositional ages ranging from ca. 273 to 261 Ma (Fig. 8). Sample 19MC-017 shows a younger peak at ca. 248 Ma (Fig. 8b), but CA-TIMS dating of 12 zircon grains across the range of LA-ICPMS dates yielded equivalent $^{206}Pb/^{238}U$ dates with a weighted mean of 262.25 Ma (Fig. 10a,b). This shows that the spread of $^{206}Pb/^{238}U$ dates in sample 19MC-017 is result of Pb loss undetected by LA-ICPMS analyses. The MDA for sample 19MC-021 was also determined by CA-TIMS at 261.51 Ma, consistent with the ca. 261 Ma peak age for that sample.
- Both igneous and detrital zircons yielded similar ranges of subchondritic εHf values between -0.5 and -23.8 (Figs. 7 and 9).
- $^{40}Ar/^{39}Ar$ dating of mica from the Sulphur Creek orthogneiss and Jim Creek pluton yielded Early Jurassic cooling ages (ca. 190-180 Ma; Fig. 12) that are consistent with previous results for this region (Fig. 11).
- The review of lithogeochemical data for Permian rocks of the western Yukon-Tanana terrane indicates a range of signatures that are consistent with emplacement in back-arc to continental arc settings.

Acknowledgments

Alfredo Camacho, University of Manitoba, produced the $^{40}Ar/^{39}Ar$ data on mica from the Jim Creek and Sulphur Creek plutons.

References

Bahlburg, H., Vervoort, J.D., and DuFrane, S.A., 2010. Plate tectonic significance of Middle Cambrian and Ordovician siliciclastic rocks of the Bavarian Facies, Armorican Terrane Assemblage, Germany — U–Pb and Hf isotope evidence from detrital zircons. Gondwana Research, vol. 17, p. 223-235.

Beranek, L.P. and Mortensen, J.K., 2011. The timing and provenance record of the Late Permian Klondike orogeny in northwestern Canada and arc-continent collision along western North America. Tectonics, vol. 30, p. 23, https://doi.org/10.1029/2010TC002849.

Blichert-Toft, J., 2008. The isotopic composition of zircon reference material 91500: Chemical Geology, vol. 253, p. 252-257.

Bouvier, A., Vervoot, J.D. and Patchett, P.J., 2008. The Lu-Hf and Sm-Nd isotopic composition of CHUR: Constraints from unequilibrated chondrites and implications for the bulk composition of terrestrial planets. Earth and Planetary Science Letters, vol. 273, p. 48-57.

Cecil, M.R., Gehrels, G.E., Ducea, M.N. and Patchett, P.J., 2011. U-Pb-Hf characterization of the central Coast Mountains batholith: Implications for petrogenesis and crustal architecture. Lithosphere, vol. 3, p. 247-260, https://doi.org/10.1130/L134.1.

Colpron, M., Nelson, J.L. and Murphy, D.C., 2006. A tectonostratigraphic framework for the pericratonic terranes of the northern Cordillera. In: Paleozoic Evolution and Metallogeny of Pericratonic Terranes at the Ancient Pacific Margin of North America, Canadian and Alaskan Cordillera, M. Colpron and J.L. Nelson (eds.), Geological Association of Canada, Special Paper 45, p. 1-23.

Colpron, M., Nelson, J.L. and Murphy, D.C., 2007. Northern Cordilleran terranes and their interactions through time. GSA Today, vol. 17, no. 4/5, p. 4-10.

Colpron, M., Israel, S., Murphy, D.C., Pigage, L.C. and Moynihan, D., 2016. Yukon Bedrock Geology Map. Yukon Geological Survey, Open File 2016-1, scale 1:1 000 000, 2 sheets, https://data.geology.gov.yk.ca/Reference/69477.

Colpron, M., McClelland, W.C., Kroeger, E.D.L., Piercey, S.J., Crowley, J.L. and Gehrels, G.E., 2025. Revisiting the “Klondike orogeny”: Permian to Jurassic development of the Yukon-Tanana terrane, northern Cordillera. Tectonics, vol. 44, https://doi.org/10.1029/2024TC008748. (in press).

Crowley, J.L., Schoene, B. and Bowring, S.A., 2007. U-Pb dating of zircon in the Bishop Tuff at the millennial scale. Geology, vol. 35, p. 1123–1126.

Dazé, A., Lee, J.K.W. and Villeneuve, M., 2003. An intercalibration study of the Fish Canyon sanidine and biotite $^{40}Ar/^{39}Ar$ standards and some comments on the age of the Fish Canyon Tuff. Chemical Geology, vol. 199, p. 111-127.

Dawson, G.M., 1899. Summary report on the operations of the geological survey for the year 1897. Geological Survey of Canada, Annual Report, vol. 10, part A, 156 p.

Dusel-Bacon, C. and Mortensen, J.K., 2023. New U-Pb geochronology and geochemistry of Paleozoic metaigneous rocks from western Yukon and eastern Alaska. U.S. Geological Survey, data release, https://doi.org/10.5066/P93ZWGA1.

Dusel-Bacon, C. and Mortensen, J.K., 2024. New U-Pb geochronology and geochemistry of Paleozoic metaigneous rocks from western Yukon and eastern Alaska, cross-border synthesis, and implications for tectonic models. U.S. Geological Survey, Professional Paper 1888, 100 p., https://doi.org/10.3133/pp1888.

Dusel-Bacon, C., Hopkins, M.J., Mortensen, J.K., Dashevsky, S.S., Bressler, J.R. and Day, W.C., 2006. Paleozoic tectonic and metallogenic evolution of the pericratonic rocks of east-central Alaska and adjacent Yukon. In: Paleozoic Evolution and Metallogeny of Pericratonic

Terranes at the Ancient Pacific Margin of North America, Canadian and Alaskan Cordillera, M. Colpron and J.L. Nelson (eds.), Geological Association of Canada, Special Paper 45, p. 25-74.

Gehrels, G.E. and Pecha, M., 2014. Detrital zircon U-Pb geochronology and Hf isotope geochemistry of Paleozoic and Triassic passive margin strata of western North America. Geosphere, vol. 10, p. 49-65.

Gehrels, G.E., Valencia, V. and Ruiz, J., 2008. Enhanced precision, accuracy, efficiency, and spatial resolution of U-Pb ages by laser ablation-multicollector-inductively coupled plasma-mass spectrometry: Geochemistry, Geophysics, Geosystems, vol. 9, Q03017, https://doi.org/10.1029/2007GC001805.

Gerstenberger, H. and Haase, G., 1997. A highly effective emitter substance for mass spectrometric Pb isotope ratio determinations. Chemical Geology, vol. 136, p. 309–312.

Gordey, S.P. and Makepeace, A.J. (comps.), 2001. Bedrock Geology, Yukon Territory; Geological Survey of Canada, Open File 3754 and Exploration and Geological Services Division, Yukon Indian and Northern Affairs Canada, Open File 2001-1, scale 1:1 000 000.

Gordey, S.P. and Ryan, J.J., 2005. Geology, Stewart River area (115N, 115O and part of 115J), Yukon Territory. Geological Survey of Canada, Open File 4970, scale 1:250 000.

Haraguchi, S., Kimura, J.-I., Senda, R., Fujinaga, K., Nakamura, K., Takaya, Y. and Ishii, T., 2017. Origin of felsic volcanism in the Izu arc intra-arc rift. Contributions to Mineralogy and Petrology, vol. 172, https://doi.org/10.1007/s00410-017-1345-1.

Hiess, J., Condon, D.J., McLean, N. and Noble, S. R., 2012. $^{238}U/^{235}U$ systematics in terrestrial uranium-bearing minerals. Science, vol. 335, p. 1610-1614.

Jaffey, A.H., Flynn, K.F., Glendenin, L.E., Bentley, W.C. and Essling, A.M., 1971. Precision measurements of half-lives and specific activities of ^{235}U and ^{238}U. Physical Review C, vol. 4, p. 1889–1906.

Kretz, R., 1983. Symbols for rock-forming minerals. American Mineralogist, vol. 68, p. 277-279.

Krogh, T.E., 1973. A low contamination method for hydrothermal decomposition of zircon and extraction of U and Pb for isotopic age determination. Geochimica et Cosmochimica Acta, vol. 37, p. 485–494.

Kuiper, K.F., Deino, A., Hilgen, F.J., Krijgsman, W., Renne, R. and Wijbrans, J.R., 2008. Synchronizing rock clocks of Earth history. Science, vol. 320, p. 500-504.

Kuiper, Y.D., Murray, D.P., Ellison, S. and Crowley, J.L., 2022. U-Pb detrital zircon analysis of sedimentary rocks of the southeastern New England Avalon terrane in the U.S. Appalachians: Evidence for a separate crustal block. In: New Developments in the Appalachian–Caledonian–Variscan Orogen. Geological Society of America, Special Paper 554, p. 93-119, https://doi.org/10.1130/2021.2554(05).

Large, R.R., Gemmell, J.B., Paulick, H. and Huston, D.L., 2001. The alteration box plot: a simple approach to understanding the relationships between alteration mineralogy and lithogeochemistry associated with VHMS deposits. Economic Geology, vol. 96, p. 957-971.

Ludwig, K.R., 2008. Isoplot 3.70 - A geochronological toolkit for Microsoft Excel. Berkeley Geochronology Center, B.G. Center, Special Publication No. 4, 76 p.

Ludwig, K.R. and Mundil, R., 2002. Extracting reliable U-Pb ages and errors from complex populations of zircons from Phanerozoic tuffs. Geochimica et Cosmochimica Acta, vol. 66, Supplement 1, p. A463, (Goldschmidt Conference Abstracts).

MacKenzie, D., Craw, D. and Mortensen, J.K., 2008. Thrust slices and associated deformation in the Klondike goldfields, Yukon. In: Yukon Exploration and Geology 2007, D.S. Emond, L.R. Blackburn, R.P. Hill and L.H. Weston (eds.), Yukon Geological Survey, p. 199-213.

Mattinson, J.M., 2005. Zircon U-Pb chemical abrasion ("CA-TIMS") method: combined annealing and multi-step partial dissolution analysis for improved precision and accuracy of zircon ages. Chemical Geology, vol. 220, p. 47–66.

Mattinson, J.M., 2010. Analysis of the relative decay constants of ^{235}U and ^{238}U by multi-step CA-TIMS measurements of closed-system natural zircon samples. Chemical Geology, vol. 275, p. 186–198, https://doi.org/10.1016/j.chemgeo.2010.05.007.

McConnell, R.G., 1905. Report on the Klondike gold fields. Geological Survey of Canada, Annual Report, vol. 14, part B, 71 p.

Milidragovic, D., Ryan, J.J., Zagorevski, A. and Piercey, S.J., 2016. Geochemistry of Permian rocks of the Yukon-Tanana terrane, western Yukon: GEM 2 Cordillera project. Geological Survey of Canada, Open File 8170, 21 p.

Min, K., Mundil, R., Renne, P.R. and Ludwig, K.R., 2000. A test for systematic errors in $^{40}Ar/^{39}Ar$ geochronology through comparison with U/Pb analysis of a 1.1-Ga rhyolite. Geochimica Cosmochimica Acta, vol. 64, p. 73-98.

Mortensen, J.K., 1988a. Geology of southwestern Dawson map area (NTS 116 B, C). Geological Survey of Canada, Open File 1927, scale 1:250 000.

Mortensen, J.K., 1988b. Geology of southwestern Dawson map area, Yukon Territory (NTS 116 B, C). In: Current Research, Part E, Geological Survey of Canada, Paper 88-1E, p. 73-78.

Mortensen, J.K., 1990. Geology and U-Pb geochronology of the Klondike District, west-central Yukon. Canadian Journal of Earth Sciences, vol. 27, p. 903-914.

Mortensen, J.K., 1992. Pre-Mid-Mesozoic tectonic evolution of the Yukon-Tanana terrane, Yukon and Alaska. Tectonics, vol. 11, p. 836-853.

Mortensen, J.K., 1996. Geological compilation maps of the northern Stewart River map area, Klondike and Sixtymile districts (115 N/15,16; 115 O/13,14 and parts of 115 O/15,16). Yukon Geological Survey, Open File 1996-1(G), scale 1:50 000, 6 maps and report.

Nelson, J.L., Colpron, M., Piercey, S.J., Dusel-Bacon, C., Murphy, D.C. and Roots, C.F., 2006. Paleozoic tectonic and metallogenic evolution of the pericratonic terranes in Yukon, northern British Columbia and eastern Alaska. In: Paleozoic Evolution and Metallogeny of Pericratonic Terranes at the Ancient Pacific Margin of North America, Canadian and Alaskan Cordillera, M. Colpron and J.L. Nelson (eds.), Geological Association of Canada, Special Paper 45, p. 323-360.

Paces, J.B. and Miller, J.D., Jr., 1993. Precise U-Pb ages of Duluth complex and related mafic intrusions, northeastern Minnesota: Geochronological insights to physical, petrogenetic, paleomagnetic, and tectonomagmatic processes associated with the 1.1 Ga midcontinent rift system. Journal of Geophysical Research: Solid Earth, vol. 98(B8), p. 13997-14013.

Pearce, J.A., 1996. A user's guide to basalt discrimination diagrams. In: Trace element geochemistry of volcanic rocks: Applications for massive sulphide exploration, D.A. Wyman (ed.), Geological Association of Canada, Short Course Notes, vol. 12, p. 79-113.

Pearce, J.A., 2014. Immobile element fingerprinting of ophiolites. Elements, vol. 10, p. 101-108, https://doi.org/10.2113/gselements.10.2.101.

Pearce, J.A. and Peate, D.W., 1995. Tectonic implications of the composition of volcanic arc magmas. Annual Reviews of Earth and Planetary Science, vol. 23, p. 251-285.

Pearce, J.A. and Stern, R.J., 2006. Origin of Back-Arc Basin Magmas: Trace Element and Isotope Perspectives. In: Back-Arc Spreading Systems: Geological, Biological, Chemical, and Physical Interactions, p. 63-86, https://doi.org/10.1029/166GM06.

Pearce, J.A., Harris, N.B.W. and Tindle, A.G., 1984. Trace element discrimination diagrams for the tectonic interpretation of granitic rocks. Journal of Petrology, vol. 25, p. 956-983.

Pearce, J.A., Baker, P.E., Harvey, P.K. and Luff, I.W., 1995. Geochemical Evidence for Subduction Fluxes, Mantle Melting and Fractional Crystallization Beneath the South Sandwich Island Arc. J. Petrology, vol. 36, p. 1073-1109, https://doi.org/10.1093/petrology/36.4.1073.

Piercey, S.J., Nelson, J.L., Colpron, M., Dusel-Bacon, C., Simard, R.-L. and Roots, C.F., 2006. Paleozoic magmatism and crustal recycling along the ancient Pacific margin of North America, northern Cordillera. In: Paleozoic Evolution and Metallogeny of Pericratonic Terranes at the Ancient Pacific Margin of North America, Canadian and Alaskan Cordillera, M. Colpron and J.L. Nelson (eds.), Geological Association of Canada, Geological Association of Canada Special Paper 45, p. 281-322.

Renne, P.R., Cassata, W.S. and Morgan, L.E., 2009. The isotopic composition of atmospheric argon and $^{40}Ar/^{39}Ar$ geochronology: time for a change? Quaternary Geochronology, vol. 4, p. 288-298.

Renne, P.R. and Norman, E.B., 2001. Determination of the half-life of ^{40}Ar by mass spectrometry. Physical Review C, vol. 63, 047302, 3 p.

Renne P.R., Swisher C.C., Deino A.L., Karner D.B., Owens T.L. and DePaolo D.J., 1998. Intercalibration of standards, absolute ages and uncertainties in 40Ar/39Ar dating. Chemical Geology, vol. 145, p. 117-152.

Roddick, J.C., 1983. High precision intercalibration of $^{40}Ar/39Ar$ standards. Geochimica Cosmochimica Acta, vol. 47, p. 887-898.

Ross, J., 2019. NMGRL/pychron v18.2, https://doi.org/10.5281/zenodo.3237834.

Ross, P.-S. and Bedard, J.H., 2009. Magmatic affinity of modern and ancient subalkaline volcanic rocks determined from trace-element discriminant diagrams. Canadian Journal of Earth Sciences, vol. 46, p. 823-839.

Ruks, T.W., Piercey, S.J., Ryan, J.J., Villeneuve, M.E. and Creaser, R.A., 2006. Mid- to late Paleozoic K-feldspar augen granitoids of the Yukon-Tanana terrane, Yukon, Canada: Implications for crustal growth and tectonic evolution of the northern Cordillera. Geological Society of America Bulletin, vol. 118, p. 1212-1231, https://doi.org/10.1130/b25854.1.

Ryan, J.J., Zagorevski, A. and Piercey, S.J., 2018. Geochemical data of Yukon-Tanana and Slide Mountain terranes and their successor rocks in Yukon and northern British Columbia. Geological Survey of Canada, Open File 8500, 11 p.

Schmitz, M.D. and Schoene, B., 2007. Derivation of isotope ratios, errors and error correlations for U-Pb geochronology using ^{205}Pb-^{235}U-(^{233}U)-spiked isotope dilution thermal ionization mass spectrometric data. Geochemistry, Geophysics, Geosystems (G^3), vol. 8, Q08006, https://doi.org/10.1029/2006GC001492.

Shervais, J.W., 2022. The petrogenesis of modern and ophiolitic lavas reconsidered: Ti-V and Nb-Th. Geoscience Frontiers, vol. 13, https://doi.org/10.1016/j.gsf.2021.101319.

Shukuno, H., Tamura, Y., Tani, K., Chang, Q., Suzuki, T. and Fiske, R.S., 2006. Origin of silicic magmas and the compositional gap at Sumisu submarine caldera, Izu-Bonin arc, Japan. Journal of Volcanology and Geothermal Research, vol. 156, p. 187-216.

Sláma, J., Košler, J, Condon, D.J., Crowley, J.L., Gerdes, A., Hanchar, J.M., Horstwood, M.S.A., Morris, G.A., Nasdala, L., Norberg, N., Schaltegger, U., Schoene, B., Tubrett, M.N. and Whitehouse, M.J., 2008. Plešovice zircon — A new natural reference material for U–Pb and Hf isotopic microanalysis. Chemical Geology, vol. 249. p. 1-35.

Spitz, G. and Darling, R., 1978. Major and minor element lithogeochemical anomalies surrounding the Louvem copper deposit, Val d'Or, Quebec. Canadian Journal of Earth Sciences, vol. 15, p. 1161-1169.

Steiger R.H. and Jäger E., 1977. Subcommission on geochronology: convention on the use of decay constants in geo- and cosmochronology. Earth Planetary Science Letters, vol. 36, p. 359-362.

Sun, S.S. and McDonough, W.F., 1989. Chemical and isotopic systematics of oceanic basalts: implications for Mantle composition and processes. In: Magmatism in Ocean Basins, A.D. Saunders and M.J. Norry (eds.), Geological Society of London, Special Publication 42, p. 313-345.

Sundell, K.E., Gehrels, G.E. and Pecha, M.E., 2020. Rapid U-Pb Geochronology by Laser Ablation Multi-Collector ICP-MS. Geostandards and Geoanalytical Research, vol. 45, p. 37-57, https://doi.org/10.1111/ggr.12355.

Sundell, K., Saylor, J.E. and Pecha, M., 2019. Provenance and recycling of detrital zircons from Cenozoic Altiplano strata and the crustal evolution of western South America from combined U-Pb and Lu-Hf isotopic analysis. In: Andean Tectonics, B.K. Horton and A. Folguera (eds.), Elsevier Inc., p. 363-397, https://doi.org/10.1016/B978-0-12-816009-1.00014-9.

van Staal, C.R., Zagorevski, A., McClelland, W.C., Escayola, M.P., Ryan, J.J., Parsons, A.J. and Proenza, J., 2018. Age and setting of Permian Slide Mountain terrane ophiolitic ultramaficmafic complexes in the Yukon: Implications for late Paleozoic-early Mesozoic tectonic models in the northern Canadian Cordillera. Tectonophysics, vol. 744, p. 458-483.

Watson, E.B., Wark, D.A. and Thomas, J.B., 2006. Crystallization themometers for zircon and rutile. Contributions to Mineralogy and Petrology, vol. 151, p. 413–433.

Whalen, J.B., Currie, K.L. and Chappell, B.W., 1987. A-type granites: geochemical characteristics, discrimination and petrogenesis. Contributions to Mineralogy and Petrology, vol. 95, p. 420-436.

Winchester, J.A. and Floyd, P.A., 1977. Geochemical discrimination of different magma series and their differentiation products using immobile elements. Chemical Geology, vol. 20, p. 325-343.

Woodhead, J.D. and Hergt, J.M., 2005. A preliminary appraisal of seven natural zircon reference materials for in situ Hf isotope determination. Geostandards and Geoanalytical Research, vol. 29(2), p. 183-195.

Yukon Geological Survey, 2023a. Yukon Lithogeochemistry data set. Yukon Geological Survey, http://data.geology.gov.yk.ca/Compilation/35, [accessed 11/7/2023].

Yukon Geological Survey, 2023b. Yukon Geochronology – A database of Yukon isotopic age determinations. Yukon Geological Survey, http://data.geology.gov.yk.ca/Compilation/22, [accessed 12/21/2023].

Yukon Geological Survey, 2024. A digital atlas of terranes for the northern Cordillera. Yukon Geological Survey, http://data.geology.gov.yk.ca/Compilation/2, [accessed 9/9/2024]

Appendices (digital)

Appendix A

Detrital zircon LA-ICPMS U-Pb geochronology data, Arizona LaserChron Centre (Microsoft Office Excel workbook).

Appendix B

LA-ICPMS isotopic U-Pb and trace element concentration data, and cathodoluminescence images for igneous zircon analyzed at the Isotope Geology Laboratory, Boise State University (Microsoft Office Excel workbooks and PDF files).

Appendix C

CA-TIMS zircon U-Pb isotopic data, Isotope Geology Laboratory, Boise State University (Microsoft Office Excel workbook).

Appendix D

LA-ICPMS Lu-Hf isotopic data, Arizona LaserChron Centre (Microsoft Office Excel workbook).

Appendix E

$^{40}Ar/^{39}Ar$ analytical data, University of Manitoba (Microsoft Office Excel workbook).

Appendix F

Compilation of lithogeochemical data for Permian rocks of the western Yukon-Tanana terrane (Microsoft Office Excel workbook).

Yukon Geological Survey
Energy, Mines and Resources
Government of Yukon